Biological methane removal by groundwater trickling biofiltration for emissions reduction

Corbera-Rubio, Francesc; Boersma, Alje S.; de Vet, Weren; Pabst, Martin; van der Wielen, Paul W.J.J.; van Kessel, Maartje A.H.J.; van Loosdrecht, Mark C.M.; van Halem, Doris; Lücker, Sebastian; Laureni, Michele

DOI
10.1016/j.watres.2025.123450

Publication date
2025

Document Version
Final published version

Published in
Water Research

Citation (APA)
Corbera-Rubio, F., Boersma, A. S., de Vet, W., Pabst, M., van der Wielen, P. W. J. J., van Kessel, M. A. H. J., van Loosdrecht, M. C. M., van Halem, D., Lücker, S., & Laureni, M. (2025). Biological methane removal by groundwater trickling biofiltration for emissions reduction. *Water Research*, *279*, Article 123450. https://doi.org/10.1016/j.watres.2025.123450

Water Research 279 (2025) 123450

Contents lists available at ScienceDirect

Water Research

journal homepage: www.elsevier.com/locate/watres

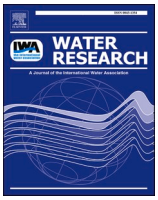

Biological methane removal by groundwater trickling biofiltration for emissions reduction

Francesc Corbera-Rubio [a,1], Alje S. Boersma [b,1], Weren de Vet [a,c], Martin Pabst [a], Paul W.J.J. van der Wielen [d,e], Maartje A.H.J. van Kessel [b], Mark C.M. van Loosdrecht [a,f], Doris van Halem [a], Sebastian Lücker [b,2,*], Michele Laureni [a,2,*]

[a] Delft University of Technology, van der Maasweg 9, Delft 2629 HZ, the Netherlands
[b] Department of Microbiology, RIBES, Radboud University, Heyendaalseweg 135, Nijmegen 6525 AJ, the Netherlands
[c] NV WML, Limburglaan 25, Maastricht 6229 GA, the Netherlands
[d] KWR Water Research Institute, P.O. Box 1072, Nieuwegein 3430 BB, the Netherlands
[e] Laboratory of Microbiology, Wageningen University & Research, Stippeneng 4, Wageningen 6708 WE, the Netherlands
[f] Center for Microbial Communities, Aalborg University, Aalborg, Denmark

ARTICLE INFO

Keywords:
Rapid sand filtration
Metaproteomics
Metagenomics
Microbial competition
Drinking water treatment

ABSTRACT

Methane removal is an essential step in drinking water production from methane-rich groundwaters. Conventional aeration-based stripping results in significant direct methane emissions, contributing up to one-third of a treatment plant's total carbon footprint. To address this, a full-scale trickling filter was operated for biological methane oxidation upstream of a submerged sand filter, and its performance was compared to a conventional aeration–submerged sand filtration set-up. Full-scale data were combined with *ex-situ* batch assays and metagenome-resolved metaproteomics to quantify the individual contribution of the main (a)biotic processes and characterize the enriched microbial communities. Both treatment setups fully removed methane, iron, ammonium, and manganese, yet the underlying mechanisms differed significantly. Methane was completely removed from the effluent after trickling filtration, with stripping and biological oxidation each accounting for half of the removal, thereby halving overall methane emissions. Methane-oxidizing bacteria not only outcompeted nitrifiers in the trickling filter, but also likely contributed directly to ammonia oxidation. In contrast to the submerged filter preceded by methane stripping, signatures of biological iron oxidation were almost completely absent in the trickling filter, suggesting that the presence of methane directly or indirectly promotes chemical iron oxidation. All systems had similar *ex-situ* manganese oxidation capacities, yet removal occurred only in the submerged filters but not the trickling filter. Ultimately, our results demonstrate that trickling filtration is effective in promoting biological methane oxidation at comparable produced drinking water quality, highlighting its potential for advancing sustainable drinking water production.

List of abbreviations

RSF	rapid sand filter
TF	trickling filter
DWTP	drinking water treatment plant

1. Introduction

Submerged sand filtration, preceded by aeration, is the most prevalent groundwater treatment technology for drinking water production in the Netherlands (Vries et al., 2017). The groundwater is aerated to strip undesired gases like methane (CH_4), hydrogen sulfide (H_2S), and carbon dioxide (CO_2), and to introduce oxygen (O_2). The introduction of O_2 to saturation levels onsets the oxidation of the main groundwater

* Corresponding authors.
E-mail addresses: s.luecker@science.ru.nl (S. Lücker), m.laureni@tudelft.nl (M. Laureni).
[1] These authors contributed equally to this work.
[2] These authors contributed equally to this work.

https://doi.org/10.1016/j.watres.2025.123450
Received 14 September 2024; Received in revised form 26 January 2025; Accepted 5 March 2025
Available online 6 March 2025

contaminants – soluble iron (Fe^{2+}), ammonium (NH_4^+), and manganese (Mn^{2+}) – in the sand filter (Bourgine et al., 1994). This treatment scheme has proven efficient and robust and provides an eco-friendly, chemical-free alternative to chlorine- and ozone-based technologies. However, methane stripping during aeration is of environmental concern due to the direct emission of this greenhouse gas to the atmosphere and can account for over a third of the carbon footprint of a drinking water treatment plant (DWTP) (Vitens, 2022). Reducing methane emissions is thus paramount to the transition towards sustainable, resource-efficient groundwater treatment systems.

Biological methane oxidation is a promising alternative to decrease direct methane emissions from DWTPs (Jiang et al., 2010). Under aerobic conditions, methane oxidation to CO_2 is performed by methane-oxidizing bacteria (MOB) (Hanson and Hanson, 1996). Aerobic MOB conserve energy from the step-wise oxidation of CH_4 to CO_2. The first step of the reaction - the transfer of one oxygen atom from O_2 to CH_4 to form methanol (CH_3OH) - is carried out by either a soluble (sMMO) or a particulate methane monooxygenase (pMMO) (Stein et al., 2012). The pMMO belongs to a protein family known as copper membrane monooxygenases (CuMMO), which also includes the ammonia monooxygenase (AMO). AMO catalyzes the oxidation of ammonia to hydroxylamine and is encoded by canonical ammonia-oxidizing bacteria (AOB) and archaea (AOA), and complete ammonia oxidizers (comammox) (Van Kessel et al., 2015; Daims et al., 2015; Stein et al., 2012). As methane and ammonia are structurally similar molecules, pMMO and AMO can catalize the oxidation of the other enzyme's primary substrate (Stein et al., 2012). Recently, MOB have even been suggested to play an important role in the nitrogen cycle in environments with high ammonium concentrations (Versantvoort et al., 2020).

Since methane removal is never complete during the aeration step, MOB are regularly found in rapid sand filters (Haukelidsaeter et al., 2023; Poghosyan et al., 2020; Palomo et al., 2016). Yet their role is poorly understood and their presence is considered undesirable (de Vet et al., 2010). The reluctance to promote the growth of MOB within sand filters stems from three distinct challenges. (*i*) High residual methane concentrations can lead to large biomass accumulations due to the high growth yields of MOB (Leak and Dalton, 1986) and extracellular polymeric substances (EPS) production (Malashenko et al., 2001). This accelerates filter clogging, shortening cycle runtimes and forcing frequent backwashing. (*ii*) The complete oxidation of 1 mol CH_4 to CO_2 requires 2 mol O_2. Sand filters often operate close to oxygen limitation, as groundwater ammonium concentrations may reach 2 mg L^{-1}. Incorporating biological methane removal could thus potentially hinder the full oxidation of some contaminants and lead to anoxic zone formation in the lower filter sections, which may promote the reduction and solubilization of previously oxidized contaminants such as manganese (Søborg et al., 2015). (*iii*) Sand filters are oligotrophic systems. Phosphate (Van der Aa et al., 2002) and copper (Wagner et al., 2016) limitation are well-known problems hindering optimal filter performance. Incorporating MOB would increase the competition for these and other (micro) nutrients, potentially compromising ammonia oxidation and biological iron and manganese removal (see (Corbera-Rubio et al., 2024a) for an overview of the reactions taking place in sand filters).

In this work, we hypothesize that the implementation of trickling filters as pre-treatment allows the promotion of biological methane oxidation without compromising the quality of the produced drinking water. Trickling filters have proven efficient in treating substrate-rich groundwaters, i.e., featuring ammonium concentrations as high as 4.5 mg NH_4^+-N L^{-1} (de Vet et al., 2009), and minimize potential oxygen limitation problems by operating at higher air-to-water ratios. To this end, we compare the performance of a novel configuration consisting of a full-scale trickling filter followed by a submerged filter with a conventional system comprising two submerged filters in series preceded by an aeration step. We assess filter performance by quantifying the removal of the main groundwater contaminants, methane, iron, ammonium, and manganese. *Ex-situ* batch incubations are used to estimate the maximum removal rates of ammonium and manganese and to assess the impact of methane on nitrification. Analyses of conversion kinetics are complemented with metagenome-resolved metaproteomics to profile the taxonomy and metabolism of the underlying microbial communities along the filters' depths.

2. Materials and methods

2.1. Operational characterization and sample collection

Filter media, water, and gas samples were collected from two groundwater-fed treatment lanes in the Breehei drinking water treatment plant (DWTP) located in Leunen, The Netherlands, and operated by NV Waterleiding Maatschappij Limburg (WML) (Fig. 1, Table 1). The first system consists of a tower aerator followed by parallel submerged filters (SF), a subsequent tower aerator, and a second set of submerged sand filters (after submerged filter; ASF). The second system does not include a tower aerator. Instead, the water is sprayed directly onto a trickling filter (TF) and air is forced in a co-current through the filter bed. Subsequently, the water passes through a tower aerator and a submerged sand filter (after tricking filter; ATF). The filter bed in each filter had a depth of 2 m. In November 2020, filter media was sampled for omics analyses and batch assays with a peat sampler at 15, 90, and 190 cm from the filter top, referred to as top (t), middle (m), and bottom (b), respectively (Fig. 1). Samples were taken at the end of the operational cycle, just before backwashing. Influent, effluent, and filter bed porewater samples were immediately filtered using 0.45 μm Millex PVDF filters (Sigma Aldrich, Saint Louis, Missouri USA), stored at 4 °C, and measured within 12 h. Porewater sampling from the trickling filter was technically not possible. Samples for total iron and manganese quantification were acidified to pH < 1 with 69 % ultrapure nitric acid. During the period of January 2020 to April 2023, dissolved O_2 concentration, pH, temperature, and redox potential were measured on-site using a multimeter (Multi 3630 IDS, Xylem Analytics, Germany). Gas flow was measured with a pressure transmitter SITRANS P320 (Siemens, Germany). Methane concentrations in the gas streams were measured using a gas chromatograph with a flame ionization detector (Agilent Intuvo 9000, Agilent Technologies, United States). To measure methane concentrations in the water streams, water samples were collected in sealed flasks and equilibrated at 25 °C under laboratory conditions. Methane concentrations in the gas phase were quantified as described above, and the concentration of methane in the water phase was calculated using using the water-to-headspace ratio and the equilibrium constant between phases of 0.0014 mol kg^{-1} bar^{-1} at 25 °C (Table 1) (Sander, 2015). The total methane content in the original water sample was then determined by summing the methane quantities in the gas and water phases. The biological methane consumption [g h^{-1}] was calculated as:

$$R_{CH_4} = \left(Q_{G,in} * C_{CH4\,G,in} + Q_{W,in} * C_{CH4\,W\,in}\right) - \left(Q_{G,out} * C_{CH4\,G,out} + Q_{W,out} * C_{CH4\,W,out}\right)$$

where Q = flow of gas (G) or water (W) [m^3 h^{-1}] and C_{CH4} = methane concentration [g m^{-3}]. Data can be found in Table S1.

2.2. Ex-situ ammonium and manganese maximum removal rates

The maximum ammonium and manganese removal rates of the filter media were determined *ex-situ* in batch. 4 g of wet filter media, 200 mL of tap water, and 100 μl of trace element solution (L^{-1}; 15 g EDTA, 4.5 g $ZnSO_4 \cdot 7H_2O$, 4.5 g $CaCl_2 \cdot 2H_2O$, 3 g $FeSO_4 \cdot 7H_2O$, 1 g H_3BO_3, 0.84 g $MnCl_2 \cdot 2H_2O$, 0.3 g $CoCl_2 \cdot 6H_2O$, 0.3 g $CuSO_4 \cdot 5H_2O$, 0.4 g $Na_2MoO_4 \cdot 2H_2O$, 0.1 g KI) were mixed in 300 mL shake flasks. After an acclimatization period of 30 min at 25°C and 150 rpm, each flask was spiked with 3 ml of 100 mg NH_4^+-N L^{-1} NH_4Cl or 100 mg Mn^{2+} L^{-1} $MnCl_2 \cdot 4H_2O$ (Sigma Aldrich, Saint Louis, Missouri USA) to reach a

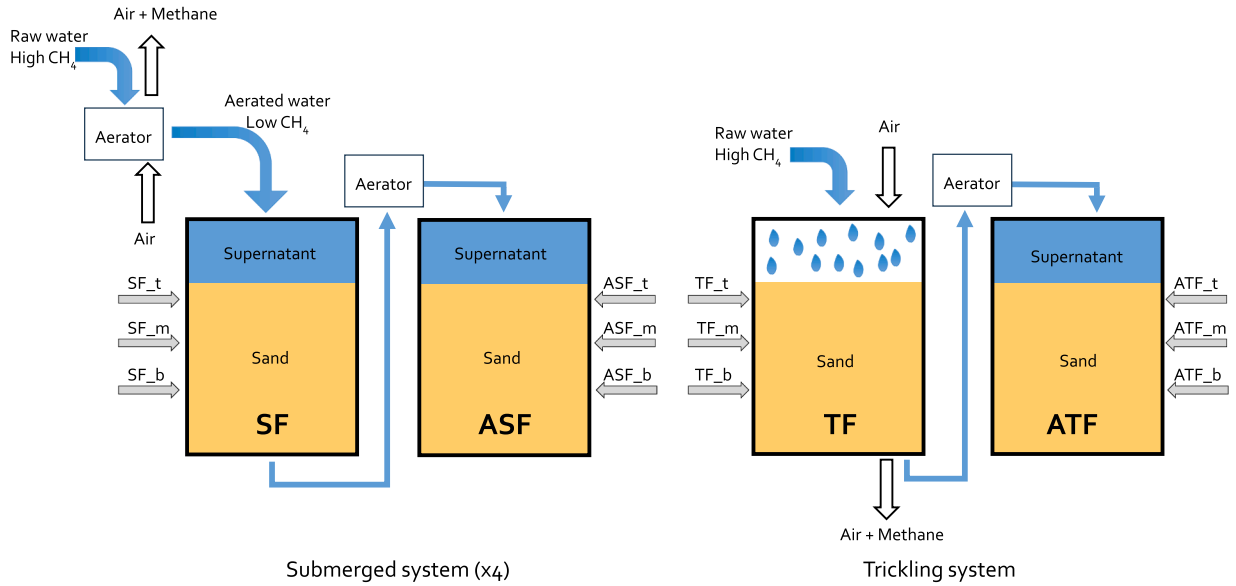

Fig. 1. Schematic illustration of the two groundwater treatment lanes. Groundwater fed into the submerged system is pre-aerated in a tower aerator, removing methane and carbon dioxide and introducing oxygen. The trickling system has no tower aerator and dissolved methane directly enters the filter. Aeration is achieved by spraying the water onto the trickling filter and forcing air in co-current through the filter bed. Each filter was characterized at three different depths: top (t), middle (m), and bottom (b) at 15 cm, 90 cm, and 190 cm from the filter top, respectively. SF, submerged filter; ASF, after submerged filter; TF, trickling filter; ATF, after trickling filter. The submerged systems consist of four parallel pre-filters and after-filters. For some of the analysis in this work, we sampled two parallel pre-filters, denoted as SF1 and SF2. Unless explicitly mentioned, SF refers to SF1.

Table 1
Operational parameters of the DWTP and the characteristics of the raw groundwater and the submerged (SF, ASF) and trickling (TF, ATF) filter lanes. Groundwater characteristics indicate the average and standard deviation of the measurements taken between January 2020 and April 2023. Oxidation-reduction potential (ORP) was measured only once.

	Unit	Submerged filters	Trickling filter
Filter depth	m	2	2
Height of supernatant	m	0.3	-
Age of media (sampling day)	years	<1	<1
Filter area	m2	9.1	
Filtration rate	m h-1	5.1	
Air-water ratio (vol./vol.)	-	-	5
Run cycle capacity	m3	1800	2500
		Groundwater	
pH		6.93 ± 0.04	
Temperature	°C	11.2 ± 0.4	
ORP	mV	-250	

concentration of 1.5 mg L^{-1}. Liquid samples (1 ml) were taken at different time intervals throughout the incubation experiment. Maximum removal rates per mass (wet weight) of filter media were calculated by interpolation of the concentration profiles and converted into volumetric rates using the measured filter media densities (2 g cm^{-3}). For the tests with methane, 1 g of wet filter media, 50 mL of tap water, and 25 µL of trace element solution were added to 110 mL sealed flasks. 5, 10, or 15 mL of methane gas (>99 % purity; Linde, Dublin, Ireland) were introduced before the addition of ammonium.

2.3. Water quality analyses

Samples for ammonium, nitrite, nitrate, and dissolved iron and manganese quantification were immediately filtered through a 0.2 µm nanopore cellulose filter (Sigma Aldrich, Saint Louis, Missouri USA) and measured within 12 h. Raw water samples were filtered after a minimum of 16 h of acidification for total iron and manganese quantification. Ammonium, nitrite, and nitrate were measured using a photometric analyzer (Gallery Discrete Analyzer, Thermo Fischer Scientific, Waltham, Massachusetts, USA). Iron and manganese were quantified by ICP-MS (Analytik Jena, Jena, Germany).

2.4. DNA extraction and sequencing

DNA was isolated from 0.5 g of filter sand (wet weight) using the DNeasy Powersoil DNA isolation kit (QIAGEN, Hilden, Germany). Cell lysis was performed by bead beating at 50 Hz for 1 min using a TissueLyser LT (QIAGEN, Hilden, Germany). When this approach yielded insufficient quantities of DNA, duplicates of 0.5 g filter sand were used and pooled on one GeneJet Spin Column. All sequencing was performed by Macrogen Inc. (Seoul, South Korea) using the Illumina MiSeq platform for 16S rRNA gene amplicon sequencing and the HiSeq platform for metagenomic sequencing. Primers used for bacterial 16S rRNA gene amplification were 341F (5′-CCTACGGGNGGCWGCAG-3′ (Herlemann et al., 2011)) and 806R (5′-GGACTACHVGGGTWTCTAAT-3′ (Caporaso et al., 2012)). Paired-end libraries were constructed using the Herculase II Fusion DNA Polymerase Nextera XT Index Kit V2 (Illumina, San Diego, USA) with the 16S Metagenomic Sequencing Library Preparation Part # 15044223 Rev. B protocol, yielding 74,000-125,000 paired-end reads per sample. For metagenomic sequencing, paired-end libraries were constructed using the Nextera XT DNA Library Preparation Kit (Illumina, San Diego, USA) with the Nextera XT DNA Library Prep Kit Reference Guide (15031942 v03), yielding approximately 80,000,000 reads per sample.

2.5. rRNA gene amplicon sequencing analysis

The 16S rRNA gene amplicon sequencing data was processed in R v3.5.1 using the DADA2 pipeline v1.8 (Callahan et al., 2016). The 16S rRNA gene-based taxonomy was obtained using the SILVA database v138.1 (Quast et al., 2013). The relative abundances calculated using DADA2 were analyzed using the R package Phyloseq v1.30.0 (McMurdie and Holmes, 2013).

2.6. Metagenome assembly

Using BBDuk in BBTools v37.76 (https://jgi.doe.gov/data-and-tools/software-tools/bbtools/), metagenomic paired-end reads with a minimal length of 75 base pairs (bp) were filtered for quality and contamination, and adapters were removed. Trimmed reads from each sample were assembled separately using metaSPAdes v3.15.4 (Nurk et al., 2017), except for reads from SF1 and SF2, which were co-assembled. K-mer sizes of 21, 33, 55, 77, and 99 were used for assembly. Only contigs $\geq$ 1000 base pairs (bp) were retained for subsequent analyses.

2.7. Metagenome binning

Reads of each sample were mapped to every assembly using BBmap (BBTools v37.76; https://jgi.doe.gov/data-and-tools/software-tools/bbtools/) to generate differential coverage data. This data was converted from sequence alignment map (SAM) files to binary alignment map (BAM) files using SAMtools v1.8 (Li et al., 2009). Differential coverage binning was performed using BinSanity v0.2.6.3 (Graham et al., 2017), CONCOCT v0.4.1 (Alneberg et al., 2013), MaxBin2 v2.2.7 (Wu et al., 2016), and MetaBat2 v2.12.1 (Kang et al., 2019), after which Das Tool v1.1.1 (Sieber et al., 2018) was used for consensus binning. Bins were dereplicated using dRep (Olm et al., 2017), using an average nucleotide identity (ANI) of 99 % for clustering. Dereplicated bins were manually refined in the Anvi'o interactive environment v7.1 (Eren et al., 2020). The completeness and contamination of bins were estimated using CheckM2 v0.1.3 (Chklovski et al., 2023) and the resulting metagenome-assembled genomes (MAGs) were defined as medium quality ($\geq$ 70 % completeness and $\leq$ 10 % redundancy) or high quality ($\geq$ 90 % completeness, $\leq$ 5 % redundancy, presence of 5S, 16S, and 23S rRNA genes, and at least 18 tRNAs) according to MIMAG standards (Bowers et al., 2017). The taxonomy of MAGs was computed using GTDBtk v2.1.1 (Chaumeil et al., 2022), and relative abundance data was generated with CoverM v0.4.0 (https://github.com/wwood/CoverM).

2.8. Functional annotation

Gene annotation was performed using DRAM v1.2.3 (Shaffer et al., 2020). Iron cycling genes were predicted using FeGenie (Garber et al., 2020). The open reading frame (ORF) predictions from the DRAM pipeline, which are generated by Prodigal (Hyatt et al., 2010), were additionally mined for nitrogen cycling genes with hidden Markov models (HMMs) built for Metascan (Cremers et al., 2022). This was done to identify additional nitrite oxidoreductase alpha subunit (*nxrA*) genes, which are poorly annotated by DRAM. Coverage data of genes was calculated with CoverM v0.4.0 (https://github.com/wwood/CoverM). Reads per kbp per million mapped reads (RPKM) were used to normalize for gene size and sequencing depth.

2.9. Phylogenetic analysis

To infer the phylogeny of the *Nitrospira* MAGs, the up-to-date bacterial core gene (UBCG) pipeline was used to extract, align, and concatenate 92 single-copy core genes (Na et al., 2018). The dataset included the identified *Nitrospira* MAGs and a reference set of 260 *Nitrospira* genomes. From this alignment, a maximum-likelihood tree was calculated with FastTree v2.1.10 using the GTR+CAT model (Price et al., 2010) and 1000 bootstrap iterations. Amino acid sequences of AMO/pMMO subunits A (AmoA/PmoA) were aligned using MUSCLE (Edgar, 2004). A maximum-likelihood tree was constructed using W-IQ-TREE (Trifinopoulos et al., 2016) with the GTR+F+I+G4 model as the determined best-fit model and using 1000 ultrafast bootstrap iterations. To distinguish between NxrA and the highly similar nitrate reductase alpha subunit NarG, an alignment was made using ARB v5.5 (Ludwig et al., 2004) of 67 protein sequences identified as described above, as well as a reference dataset of 416 NxrA and NarG sequences (Poghosyan et al., 2020). A maximum-likelihood tree was constructed from this alignment using IQ-TREE v2.1.4 (Minh et al., 2020), with the Q.pfam+I+G4 model as the determined best-fit model, and using 1000 ultrafast bootstrap iterations. All trees were visualized in iTOL (Letunic and Bork, 2021)

2.10. Protein extraction, proteolytic digestion, and shotgun proteomic analysis

For protein extraction, 150 mg of filter (sand) material was mixed with 125 µL of B-PER reagent (78243, Thermo Scientific) and 125 µL 1 M TEAB buffer (50 mM TEAB, 1 % w:w NaDOC, adjusted to pH 8.0). The mixture was briefly vortexed and exposed to shaking using a Mini Bead Beater 16 (BioSpec Products) for 3 min. Afterwards, the sample was exposed to one freeze/thaw cycle at -80°C and +80°C for 15 and 5 min, respectively. The samples were centrifuged for 10 min at 10,000 rpm and 4°C, and the supernatant was transferred into a clean LoBind Eppendorf tube (Eppendorf, Hamburg, Germany). Another 125 µL of B-PER reagent and 125 µL 1 M TEAB buffer were added to the sand sample, vortexed, and sonicated (Branson 5510, sonication mode, at room temperature) for 5 min. The sample was again centrifuged for 10 min at 10,000 rpm and 4°C, and the supernatant was collected and pooled with the first supernatant. Extracted proteins were precipitated by adding 200 µL ice-cold acetone to the supernatant, vortexing, and incubation at -20°C for 1 h. The protein pellet was collected by centrifugation at 14,000 rpm and 4°C for 15 min. The supernatant was carefully removed from the pellet using a pipette. The pellet was dissolved in 100 µL 200 mM ammonium bicarbonate containing 6 M urea. Disulfide bonds were reduced using 10 mM DTT (dithiothreitol), and sulfhydryl groups were blocked using 20 mM IAA (iodoacetamide). The solution was diluted to below 1 M urea and digested using sequencing-grade Trypsin (Promega). The proteolytic peptides were finally desalted using an Oasis HLB solid phase extraction well plate (Waters) according to the manufacturer's protocol. An aliquot corresponding to approximately 250 ng of protein digest was analyzed with a shotgun proteomics approach as described earlier (Kleikamp et al., 2021, 2023). Briefly, the peptides were analyzed using a nano-liquid-chromatography system consisting of an EASY nano-LC 1200, equipped with an Acclaim PepMap RSLC RP C18 separation column (50 um × 150 mm, 2 µm, 100 Å) and a QE plus Orbitrap mass spectrometer (Thermo Fisher, Germany). The flow rate was maintained at 350 nL over a linear gradient from 5 % to 30 % solvent B over 65 min and finally to 60 % B over 20 min. Solvent A was ultrapure H_2O containing 0.1 % v:v formic acid, and solvent B consisted of 80 % acetonitrile in H_2O and 0.1 % v:v formic acid. The Orbitrap was operated in data-dependent acquisition (DDA) mode acquiring peptide signals from 385-1250 m/z at 70K resolution. The top 10 signals were isolated at a window of 2.0 m/z and fragmented at a NCE of 28 at 17.5K resolution with an AGC target of 2e5 and a max IT 75 ms. The collected mass spectrometric raw data were analyzed combined against the metagenomics reference sequence database built from the assembled contigs using PEAKS Studio 10 (Bioinformatics Solutions, Canada) in a two-round search approach. The first-round database search using the clustered database (892,436 proteins) was used to construct a focused protein sequence database, considering one missed cleavage, carbamidomethylation as fixed modification, and allowing 15 ppm parent ion and 0.02 Da fragment ion mass error. The focused database (comprising 9729 proteins) was then used in a second-round search, considering 3 missed cleavages, carbamidomethylation as fixed, and methionine oxidation and N/Q deamidation as variable modifications. Peptide spectrum matches were filtered for a 5 % false discovery rate (FDR), and protein identifications with at least 2 unique peptides were considered significant. Functional annotations (KO identifiers) and taxonomic lineages were obtained by GhostKoala (https://www.kegg.jp/ghostkoala) and by Diamond (Buchfink et al., 2014) using the NCBI nr protein sequence reference database (Index of /blast/db/FASTA (nih.gov)). For Diamond annotations, the lineage of the lowest common ancestor was

determined from the top 10 sequence alignments. Data is given in Table S2.

Comparison of the relative abundance of proteins between samples was performed using "relative spectral counts" (i.e., normalized spectral counts, defined as spectral counts per protein divided by the molecular weight of the specific protein, and normalized by the sum of mass-normalized spectral counts of all proteins of all samples). The contribution of a specific protein was estimated by summing up the relative abundances of all proteins with the same functional annotation. For proteins with more than one subunit, only the catalytic one was considered: AmoB for ammonia monooxygenase AMO, MmoX for soluble methane monooxygenase sMMO, PmoB for particulate methane monooxygenase pMMO; NarG for nitrate reductase NAR, NxrA for nitrite oxidoreductase NXR, NorB for nitric oxide reductase NOR, MtoA for iron oxidase MTO. For the putative particulate methane monooxygenase pXMO, subunit A (PxmA) was used as it was the only one present in the metaproteome.

3. Results

3.1. Complete methane and iron removal at the expense of incomplete ammonia and manganese oxidation in the trickling filter

The concentration profiles of methane, iron, ammonium, and manganese differed among the two studied treatment processes (Fig. 2). In the submerged system, virtually all (>99.9 %) methane was removed after aeration (AA) before reaching the first submerged filter (SF). Ammonia, iron, and manganese were completely removed in the SF, with effluent concentrations of < 0.1 mg Fe^{2+} L^{-1}, < 0.05 mg NH_4 L^{-1}, and < 0.5 μg Mn^{2+} L^{-1}. In the trickling system, anaerobic groundwater is directly fed to the trickling filter (TF) together with an air stream, allowing complete methane removal in the TF (> 99.5 %). Based on the influent and effluent gaseous and dissolved methane concentrations (Table S1), it was estimated that approximately 47 % was biologically oxidized, with the remaining methane being stripped. Iron was completely depleted in the trickling filter as well (effluent < 0.05 mg Fe^{2+} L^{-1}), while the oxidation of ammonium and manganese was only partial (26 % and 19 %, respectively). Total ammonium and manganese removal was achieved at the effluent of the submerged after-trickling filter (ATF; effluent < 0.05 mg NH_4^+ $L^{-1;}$ < 0.5 μg Mn^{2+} L^{-1}).

3.2. Methane controls nitrification and manganese oxidation rates in both systems

3.2.1. Ammonia and manganese removal rates

The maximum ammonium and manganese removal capacities of the filter media along the depth of all filters were quantified *ex-situ* in batch activity tests (Fig. 3). Ammonium removal was comparable in the two studied parallel submerged filters (SF1 and SF2), with a subtle top-to-bottom decreasing profile following the decrease in ammonium concentrations. Consistent with the low ammonium consumption in TF (Fig. 2A), the removal capacity at the top of TF (TF_t) was 7 times lower than in SF1_t, namely 0.26 and 1.82 g NH_4^+-N m_{media}^{-3} h^{-1}, respectively. The ammonia removal increased slightly in the lower TF sections. The subsequent submerged filter (ATF) showed the highest and most stratified ammonium removal capacity with 3.49 g NH_4^+-N m_{media}^{-3} h^{-1} at the top and 0.94 at the bottom.

Ex-situ manganese removal capacities were also comparable for SF1 and SF2, with similar rates across both filters (0.117 ± 0.007 g m_{media}^{-3} h^{-1} for SF1 and 0.107 ± 0.007 g m_{media}^{-3} h^{-1} for SF2). In analogy to ammonium, the manganese removal capacity increased towards the bottom of TF (from 0.103 ± 0.071 g m_{media}^{-3} h^{-1} at TF_t to 0.133 ± 0.000 g m_{media}^{-3} h^{-1} at TF_b). Surprisingly, the measured rates were similar to those in SF1 and SF2, despite the fact that less than 25 % of manganese

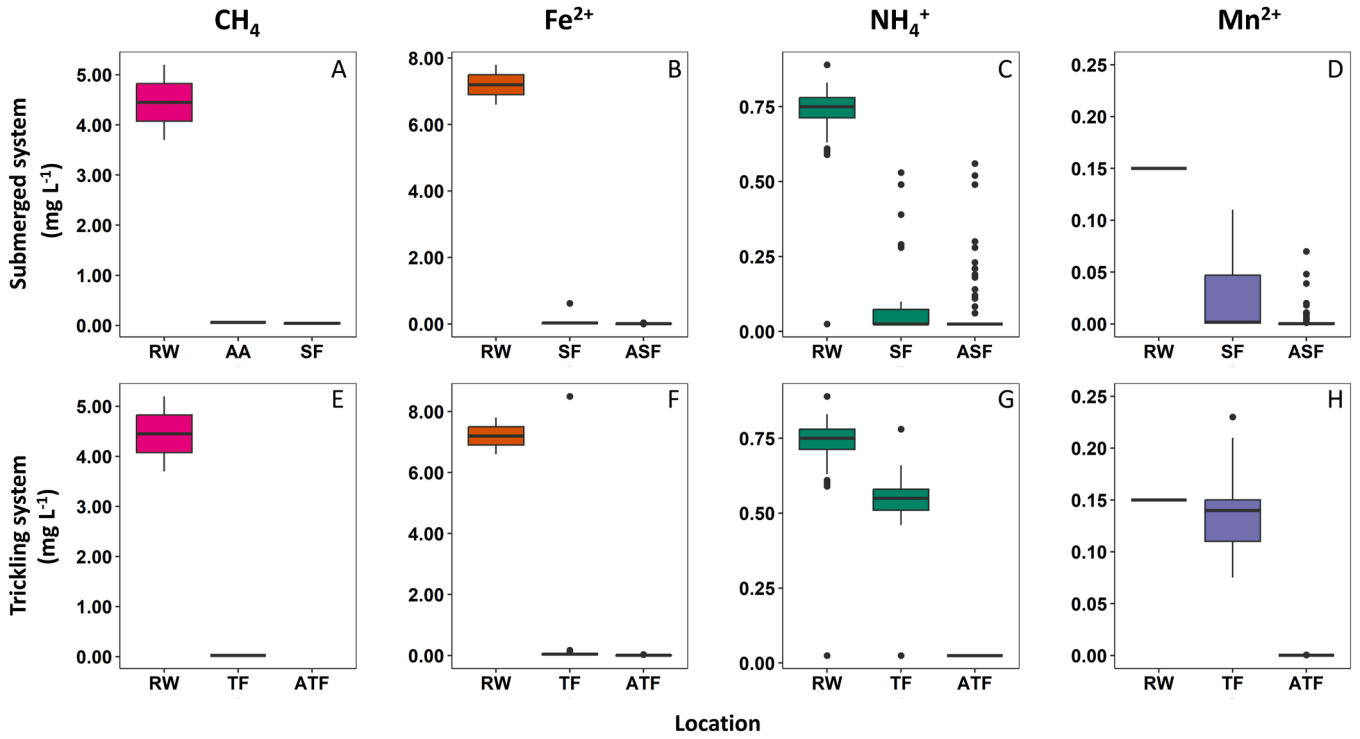

Fig. 2. Concentration profiles of methane (A,E), iron (B,F), ammonium (C,G), and manganese (D,H) along the submerged (top) and trickling systems (bottom) in DWTP Breehei. Complete removal is achieved at the end of both systems. Groundwater is aerated before reaching the submerged system, where methane is removed but the other contaminants are not. Values and error bars represent the mean and standard deviation of measurements taken between January and July 2020. Lower and upper box boundaries represent the 25th and 75th percentiles, the line inside the box is the median. Lower and upper error lines indicate 10th and 90th percentiles. Individual points show outliers, which belong to the start-up phase. RW, raw water; AA, after aeration; SF, submerged filter; ASF, after-submerged filter; TF, trickling filter; ATF, after-trickling filter.

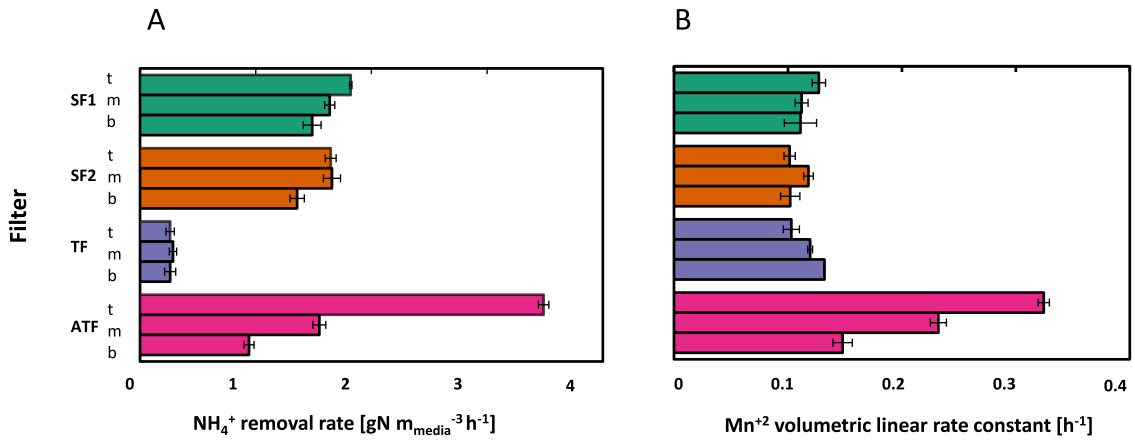

Fig. 3. Maximum volumetric *ex-situ* ammonium (a) and manganese (b) removal rates in the top (t), middle (m), and bottom (b) sections of SF1, SF2, TF, and ATF. Batch tests were carried out in duplicate, error bars represent the standard deviation. SF1 and SF2, parallel submerged filters; TF, trickling filter; ATF, after-trickling filter.

was removed in the TF while complete oxidation was observed in SF1 and SF2. Again, the highest and most stratified rates were found in the ATF, likely due to the absence of methane and iron.

3.2.2. *Methane-oxidizing bacteria's potential contribution to ammonia oxidation*

To explore the impact of methane on ammonium removal, nitrification batch tests were carried out under methane-rich atmospheres using media from the top of each filter (Fig. 4A). The presence of methane decreased the maximum ammonium removal rate of the media from the filters that do not receive methane, with reductions of 65 % in SF1, 73 % in SF2, and 60 % in ATF. In contrast, ammonium removal was 173 % higher in the presence of methane for TF media.

To further characterize the mechanisms behind this effect, we exposed sand from SF1_t and TF_t to increasing methane concentrations, using 0, 8, 14, and 20 % (v:v) methane atmospheres at a constant ammonium concentration (Fig. 4B). For the sand from the SF, higher methane concentrations resulted in proportionally lower ammonium removal rates, with a reduction from 1.14 to 0.26 g NH_4^+-N m_{media}^{-3} h^{-1} when methane increased from 0 to 20 %. Ammonium removal was accompanied by nitrite and nitrate production, consistent with full nitrification. In contrast, with TF medium, ammonium removal was the lowest at 0 % methane (0.26 g NH_4^+-N m_{media}^{-3} h^{-1}) and at comparable higher rates in the presence of 8, 14, and 20 % methane (0.96, 0.89, and 0.95 gNH_4^+-N m_{media}^{-3} h^{-1}, respectively). Nitrite production was detected at all methane concentrations, while no nitrate was produced. On the contrary, nitrate initially present in the vials was consumed in all TF tests, presumably due to denitrification. This resulted in nitrogen mass balances of < 80 %.

3.3. *Microbial community composition and genome-based functional potential*

3.3.1. *Nitrifying and iron-oxidizing guilds govern the SF, while methanotrophs dominate the TF*

The microbial community composition, elucidated through 16S rRNA gene amplicon sequencing, showed distinct differences between the submerged and trickling treatment systems (Fig. 5). In SF1 and the identically operated parallel SF2, where methane is removed by pre-aeration, the genera *Gallionella* (3-27 %) and *Nitrospira* (8-18 %) dominated the microbial communities. The communities at the middle and bottom of SF1 and SF2 were similar. Samples from the top showed greater dissimilarity (Fig. S1), primarily due to the higher prevalence of *Gallionella* in SF1 compared to SF2. In stark contrast, MOB of the genera *Methylovulum* (9-32 %) and *Crenothrix* (7-11 %) and methylotrophic bacteria of the genus *Methylotenera* (16-29 %) dominated the TF, which

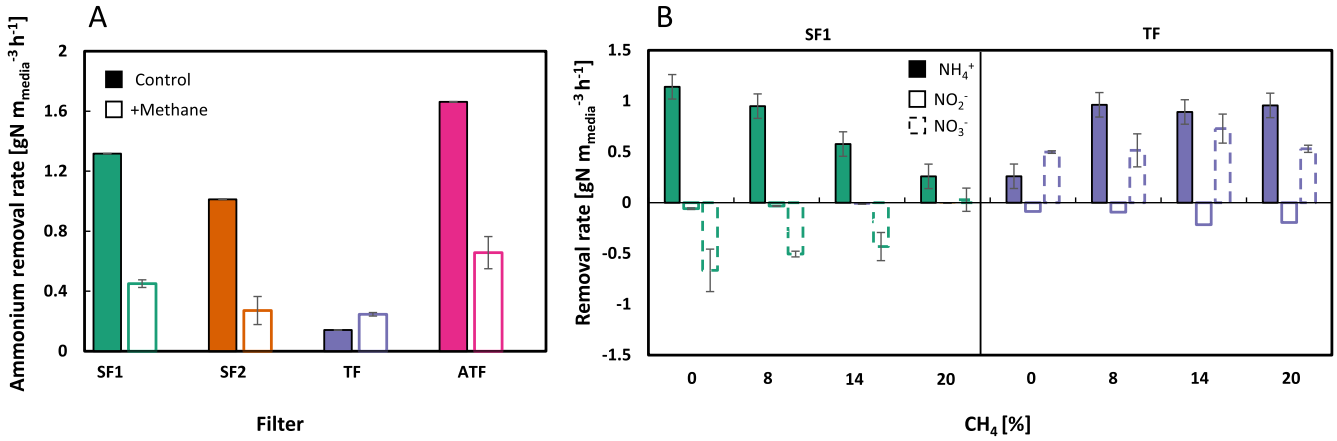

Fig. 4. Maximum volumetric *ex-situ* ammonium removal rates. A) Ammonium removal in the top section of SF1, SF2, TF, and ATF in the presence (full) or absence (empty) of a 20 % (v:v) methane atmosphere. B) Maximum volumetric *ex-situ* ammonium consumption (full), and nitrite (empty) and nitrate (empty, dotted) production rates in the top sections of SF1 and TF in the presence of 0, 8, 14, and 20 % (v:v in air) methane atmospheres. Batch tests were carried out in duplicate; error bars represent the standard deviation (in some cases smaller than symbols). SF1 and SF2, parallel submerged filters; TF, trickling filter; ATF, after-trickling filter.

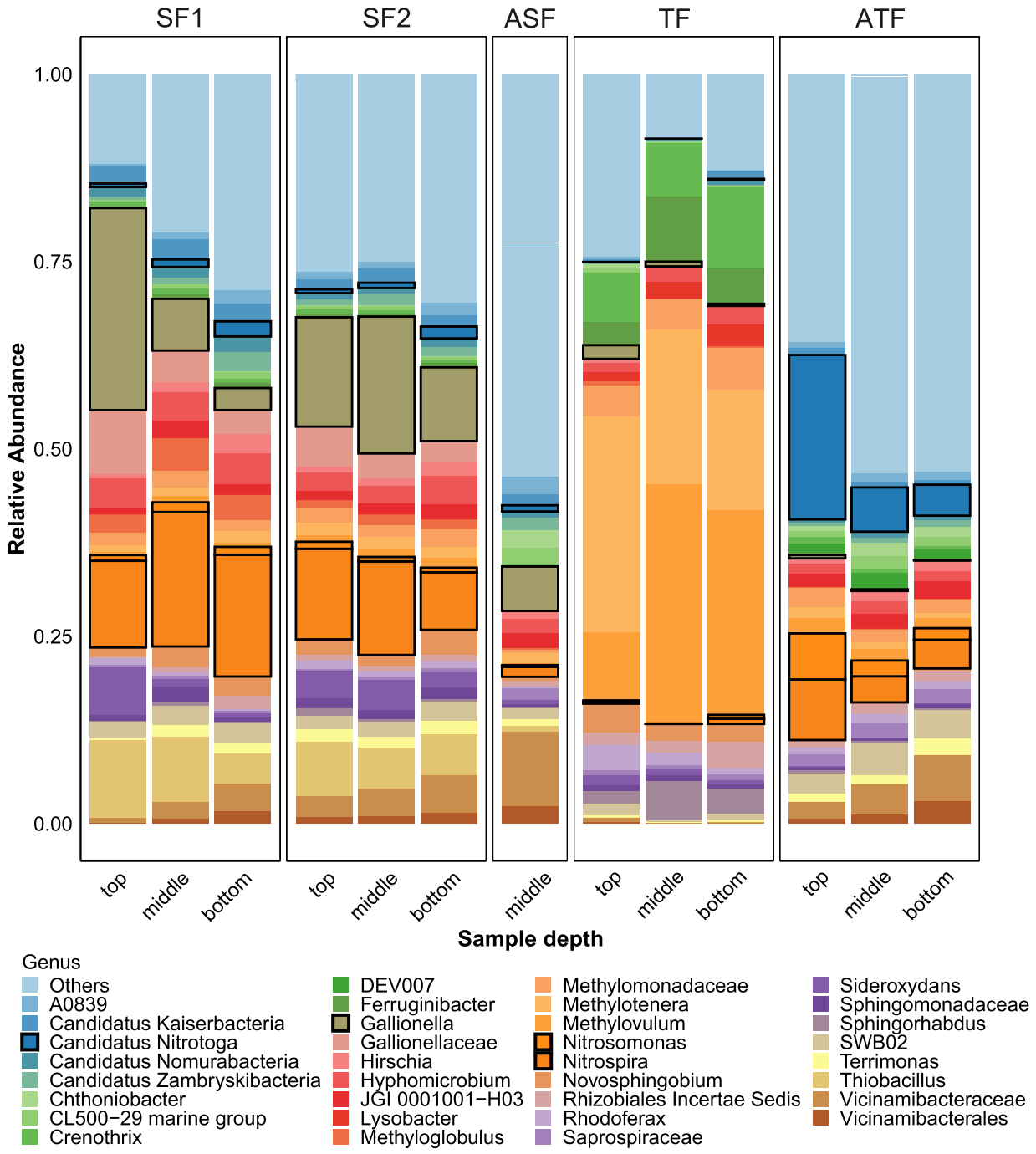

Fig. 5. Relative microbial community composition based on 16S rRNA gene amplicon sequencing. All genera constituting ≥ 2 % of the total microbial community in at least one of the samples are shown for every sample. All other taxa are grouped in 'Others'. The genera *Candidatus* Nitrotoga, *Gallionella, Nitrosomonas*, and *Nitrospira* are highlighted. SF1 and SF2, parallel submerged filters; ASF, after-submerged filter; TF, trickling filter; ATF, after-trickling filter.

directly receives methane-rich groundwater. The relative abundance of *Methylotenera* decreased from top to bottom while *Methylovulum* displayed an opposite profile (Fig. 5).

The microbial community of ASF, receiving water containing minimal residual levels of ammonium, iron, and manganese, featured a much lower abundance of taxa involved in their removal compared to the other filters (Fig. 5). The dominant ASF bacteria belonged to the genera *Vicinamibacteraceae* (10 %) and *Gallionella* (6 %). Contrastingly, the influent water of the ATF still contained high levels of ammonium and manganese, and *Candidatus* Nitrotoga (4-22 %), *Nitrospira* (4-8 %), and *Nitrosomonas* (1-6 %) were the predominant genera, particularly in the top layer.

3.3.2. *The submerged and trickling lines harbor distinct functional guilds*

The microbial community metagenome of each filter was sequenced to characterize the metabolic potential of the most abundant organisms. Sequencing yielded 79-85 million paired-end raw reads and 69-77 million trimmed reads per sample (Table S3). Of the trimmed reads, 49-85 % could be assembled into contigs, 55-83 % of which were binned into metagenome-assembled genomes (MAGs). After dereplication at strain level, 14 high and 108 medium-quality MAGs were obtained (Table S4).

The MAGs of interest were identified based on the presence of genes involved in methane, manganese, and iron oxidation, as well as nitrification and denitrification (Fig. 6). In the parallel filters SF1 and SF2, the

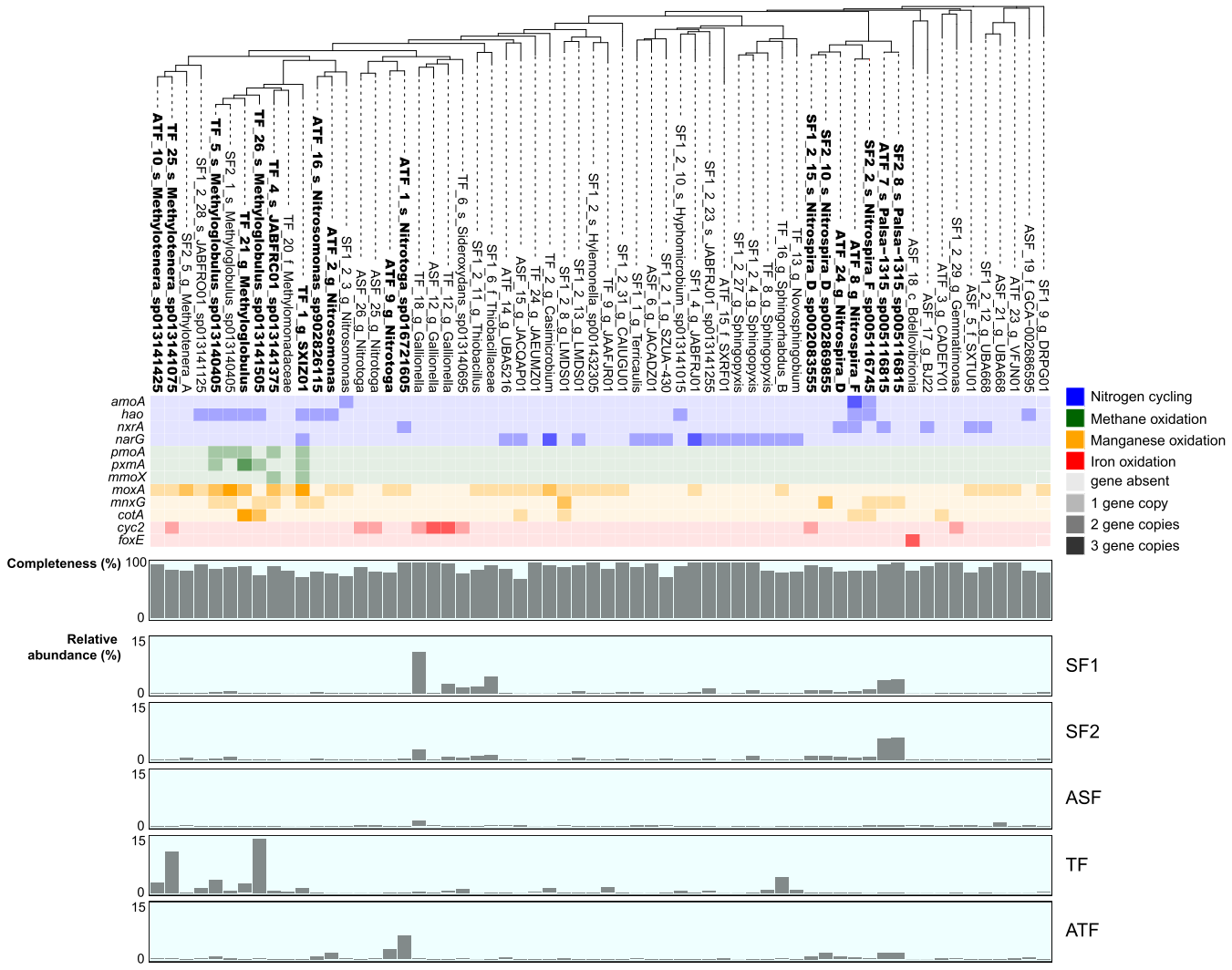

Fig. 6. Overview of phylogeny, genetic potential, completeness, and distribution of 62 dereplicated high and medium-quality MAGs. These MAGs were selected out of the total 122 medium and high-quality MAGs by the presence of genes involved in nitrogen cycling, methane, manganese, or iron oxidation. The order of the MAGs is based on the phylogeny of all 122 MAGs, as determined by a maximum-likelihood tree calculated with FastTree using the GTR+CAT model, based on the alignment of 92 single core copy genes by UBCG. Copy numbers of genes involved in nitrogen cycling, methane, manganese, and methane oxidation are shown as a heat map. Bar plots show the completeness of the MAGs (middle) and their relative abundance in the different filters (bottom). SF1 and SF2, parallel submerged filters; ASF, after-submerged filter; TF, trickling filter; ATF, after-trickling filter.

most abundant MAGs belonged to the genera *Gallionella* and *Nitrospira*, in accordance with the 16S rRNA gene amplicon sequencing. The *Gallionella* MAGs contained one or two copies of the iron oxidation gene *cyc2*, showcasing their involvement in biological iron removal. The most abundant *Nitrospira* MAGs, ATF_7 and SF2_8, did not contain the ammonium monooxygenase subunit A (*amoA)* or hydroxylamine dehydrogenase (*hao*) genes, indicating that they are canonical (nitrite-oxidizing only) *Nitrospira*. Contrastingly, *Nitrospira* MAGs ATF_8 and SF2_2 contained both *amoA* and *hao*, hence representing complete ammonia-oxidizing (comammox) species. The gene encoding the nitrite oxidoreductase subunit alpha (*nxrA*) was only found in ATF 7, ATF_8, and ATF_24. However, as *nxr* is part of the core genome of all *Nitrospira* species (Koch et al., 2019), its absence in SF2_2 (as well as in SF1_2, SF2_10, and SF2_8) is therefore attributed to MAG incompleteness.

To account for additional *amoA* copies possibly missed in the binning process resulting in *Nitrospira* MAG misclassification, the phylogeny of all *Nitrospira* MAGs and a reference dataset of 260 *Nitrospira* genomes was determined using a concatenated alignment of 92 single-copy core genes (Fig. S2). All recovered *Nitrospira* MAGs belonged to lineage II and most clustered with canonical nitrite-oxidizers. The phylogenetic analysis confirmed that ATF_8 and SF2_2 represented the only comammox species, belonging to comammox clade A. When comparing filters, comammox *Nitrospira* were more abundant in the parallel submerged systems (1.7 % in SF1 and 1.6 % SF2) than in the trickling system (0.5 % in ATF). Instead, *Candidatus* Nitrotoga (ATF_9 and ATF_1) and *Nitrosomonas* (ATF_16 and ATF_2) MAGs follow the opposite trend, constituting 0.18 and 0.32 %, and 0.33 and 0.45 % in SF1 and SF2, and 9.7 % and 2.6 % in ATF, respectively. In the ASF, the MAGs involved in methane, iron, manganese, or ammonium removal were present in low abundances.

The methanotrophic *Methyloglobulus* MAG TF_26 (15.7 %) and the methylotrophic *Methylotenera* MAG TF_25 (11.7 %) were the most abundant MAGs in the TF. TF_26 encoded *pxmA* but lacked *pmoA*. Given that *pmoA* is a critical component of the core metabolism of all aerobic methanotrophic bacteria (Knief, 2015), its absence is likely due to incomplete binning. Eight less abundant methanotrophic MAGs were also found, all of which harbored *pmoA*, complemented by *pxmA* in TF_1, TF_5, and TF_21, and by the soluble methane monooxygenase (*mmoX*) in TF_1 and TF_4.

The genetic potential for manganese oxidation, as determined by the

presence of *moxA, mnxG*, and *cotA*, was widespread across all samples and not limited to any particular group of bacteria.

3.3.3. Gene-centric analysis supports bin-centric functional distribution

While bin-centric analysis is a powerful approach to studying microbial community composition, it does not take into account unbinned genes, which may represent a significant fraction of the metagenome. Therefore, a gene-centric analysis was performed to examine the full methane and ammonia oxidation potential of the community. A phylogenetic tree of all translated copper-containing membrane monooxygenases (Cu-MMO) subunit A genes showed that the Cu-MMOs in our metagenomes cluster within five distinct groups (Fig. 7A): *i)* comammox *Nitrospira* clade A AmoA, *ii)* betaproteobacterial (*Nitrosomonadacaea*) AmoA, *iii)* ERR11-like Cu-MMO, *iv)* PxmA group, and *v)* gammaproteobacterial PmoA. Based on metagenomic read mapping, *Nitrosomonadacaea amoA* was the most abundant gene for ammonium removal across all samples, especially in ATF (Fig. 7B), followed by clade A comammox *amoA,* which represented *ca.* 30-50 % of total *amoA* in the submerged system (SF1/SF2, ASF), but only comprised a minor fraction of total *amoA* in the trickling system (TF, ATF). In the TF metagenome, no *amoA* was found, while it contained the highest abundance of methane oxidation genes, corresponding to biological methane removal being the dominant process in this filter. The most abundant gene was *pxmA* (Fig. 7C), with gammaproteobacterial *pmoA* also present. Surprisingly, gammaproteobacterial *pmoA* was found in similar abundances across all filters, despite the significant differences in methane concentrations in the incoming waters. Genes encoding *mmoX* were only obtained from the TF, and at low abundance.

A similar approach was followed to resolve the distribution of nitrite oxidoreductase and nitrate reductase alpha subunit genes (*nxrA* and *narG*, respectively; Fig. S3). In the protein-based phylogenetic analysis, these fall into four distinct groups: NarG, *Nitrospira* NxrA, *Candidatus* Nitrotoga NxrA, and putative *Nitrotoga*-like NxrA/NarG. Based on RPKM analysis, *Nitrospira nxrA* was the most abundant gene, especially in the filters where nitrification occurred (SF1, SF2, and ATF).

3.4. Protein-centric metabolic profiles

The proteomes of the top, middle, and bottom sections of SF and TF were quantified to estimate the distribution of core nitrogen, methane, iron, and manganese-transforming enzymes. Per sample, we obtained, on average, 335 ± 33 individual protein groups identified by at least two unique peptides at a false discovery rate < 1 % (Table S2). The relative contribution of individual functions of interest was estimated by grouping all proteins with the same functional annotation. Relative protein abundances were calculated as protein-mass normalized spectral counts divided by the total spectral counts of the 6 samples (Fig. 8).

The catalytic subunits of the three protein complexes involved in nitrification – ammonia monooxygenase subunit B (AmoB), hydroxylamine dehydrogenase (Hao), and nitrite oxidoreductase alpha subunit (NxrA) – were present across all sections of the SF. The abundance of AmoB was clearly stratified along the filter depth, with a larger abundance in the downstream sections. In accordance, *in situ* ammonia oxidation rates in the SF were higher in the lower bed sections, subsequent to the oxidation of most Fe^{2+} (Fig. S4). The distribution of Hao and NxrA did not follow a specific trend. Conversely, and in agreement with the near-absent ammonium conversion and lack of *amoA*, no nitrifying proteins were detected in the TF. Instead, proteins encoding for methane monooxygenases were abundant and displayed distinct distribution trends. PmoB and PxmA showed a decreasing top-to-bottom stratification, apparently following the direction of water flow. On the contrary, MmoX was only present at the bottom of the TF, yet at significant relative abundances.

Fingerprints of biological iron oxidation were only found in the SF,

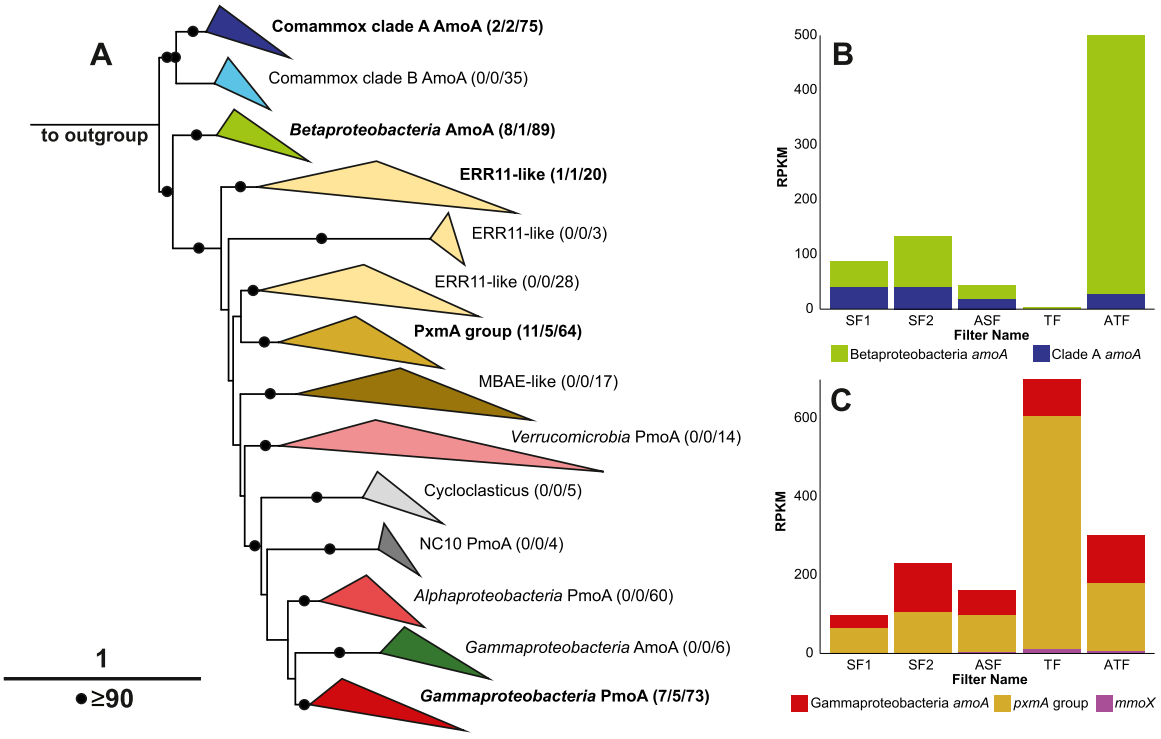

Fig. 7. Diversity and abundance of genes involved in methane and ammonia oxidation. (A) The phylogenetic tree shows the diversity of Cu-MMO proteins. Clades highlighted in bold contain sequences from the rapid sand filter metagenomes of this study. The numbers in brackets represent the number of distinct sequences from the rapid sand filter metagenomes, the number of these sequences found in MAGs, and the total count of sequences in that clade, respectively. The outgroup consists of three *Nitrososphaerota* AmoA sequences. (B, C) Abundances of betaproteobacterial *amoA* and comammox *Nitrospira* clade A *amoA* (B), and gammaproteobacterial *pmoA* and *pxmA* (C) in all filters, normalized as RPKM. Although not part of the Cu-MMO family, *mmoX* is also included due to the role of sMMO in methane oxidation. SF1 and SF2, parallel submerged filters; ASF, after-submerged filter; TF, trickling filter; ATF, after-trickling filter.

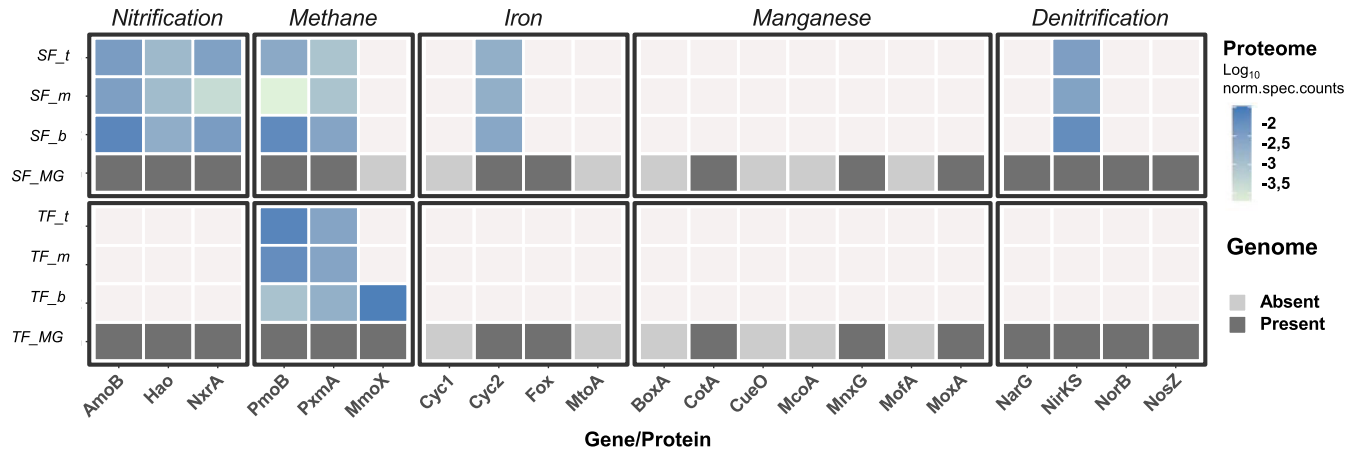

Fig. 8. Distribution of the key proteins involved in methane, iron, and manganese oxidation, nitrification, and denitrification. Relative protein abundances were calculated as protein-mass normalized spectral counts divided by the total spectral counts of the 6 samples. The key proteins were selected based on the nitrification, denitrification, and methane oxidation pathways (#M00528, #M00529, #M00174) of the Kyoto Encyclopedia of Genes and Genomes, FeGenie for iron (Garber et al., 2020), and a custom-made database for manganese oxidation (Hu et al., 2020). Dark grey: genes found at least once in the metagenome but not in the metaproteome; light grey: genes not found in the metagenome. For protein complexes, only the catalytic subunit was included. For more information, see Materials and Methods.

where Cyc2 was homogeneously present across all filter depths. These results are in line with the high and low abundances of *Gallionella* in SF and TF, respectively, based on 16S rRNA and iron oxidase Cyc2 genes (Fig. S5). For manganese removal, genes encoding for the multicopper oxidases CotA, MnxG, and MoxA were the only putative manganese oxidation genes present in the filters, but the corresponding proteins were not detected. Lastly, genes encoding the four key enzymes in denitrification – nitrate reductase (*narG*), NO-forming nitrite reductase (*nirK* or *nirS*), nitric oxide reductase (*norB*), and nitrous oxide reductase (*nosZ*) – were present in both filters. However, NirK was the only expressed protein and exclusively found in SF, where it showed similar stratification with depth as AmoB, having an increased abundance at greater depths in the filter.

4. Discussion

4.1. Biological methane oxidation during trickling filtration halves emissions at comparable effluent quality

Complete methane removal (>99.5 %) was achieved both in the trickling and submerged systems. Most methane was stripped during aeration before reaching the filters in the conventional submerged system. In contrast, all methane was removed in the TF, with about half (47 %) being biologically oxidized to carbon dioxide, and the rest being stripped. Importantly, the adoption of the new operation did not compromise the effluent water quality.

Methane-oxidizing bacteria affiliated with the genus *Methylovulum* and methylotrophic bacteria of the genus *Methylotenera* dominated the microbial population across the full depth of the TF, as indicated by 16S rRNA gene abundance (Fig. 5) and MAG-centric analysis (Fig. 6). Interestingly, *Methylotenera* was the most abundant organism at the top of the TF, while the genus *Methylovulum* dominated the downstream sections. Some *Methylotenera* species obtain energy from methylamine and methanol oxidation (Afshin et al., 2021) but none have ever been reported to consume methane. Since methane oxidation to methanol does not yield energy (Stein et al., 2012), a syntrophic relationship between *Methylotenera* and MOBs based on methanol exchange is unlikely. Thus, if *Methylotenera* rely on methanol scavenging, their surprisingly high relative abundance in the first section of the TF remains at least partially unexplained. The dominant enzyme for methane oxidation also changed throughout the filter depth. While the particulate methane monooxygenase (pMMO) was the most abundant methane oxidase at the top, its soluble counterpart (sMMO) took over in the downstream section. Interestingly, the sequence-divergent particulate methane monooxygenase pXMO (Tavormina et al., 2011) was highly abundant at both gene (Fig. 7C) and protein (Fig. 8) levels and followed the same top-to-bottom decreasing pattern as pMMO. The balance between the particulate and soluble methane monooxygenases is known to be dictated by the "copper switch" (Stanley et al., 1983), with pMMO dominating at high Cu concentrations and the iron-dependent sMMO under Cu deficiency (Murreil et al., 2000). Cu limitation is known to occur in the lower sections of sand filters (Wagner et al., 2016), so it is tempting to speculate that the observed distribution of MOB in the TF is dictated by Cu availability. However, while no Cu is dosed in between TF and ATF, *Nitrosomonas* dominated throughout the ATF depth over *Nitrospira*, which usually are enriched under Cu-limiting conditions (Wagner et al., 2016) suggesting that Cu is not limiting. Thus, further experimental evidence on the impact of Cu on MOB is warranted.

In the submerged filter, MOB and, correspondingly, PmoB were abundant despite near-complete methane removal during the preceding aeration step (<99.9 %). Proliferation of MOB in sand filters that receive aerated water supposedly devoid of methane is commonly reported (Palomo et al., 2016; Gülay et al., 2016; Poghosyan et al., 2020). Their high abundance despite the low methane concentration likely derives from their higher biomass yield (~0.7 g dry cell weight g CH_4^{-1} (Leak and Dalton, 1986)) compared to the other main microbial community members (<0.16 g dry cell weight g NH_4^+-N^{-1} for AOB (González-Cabaleiro et al., 2019); ~0.013 g dry cell weight g Fe^{-1} for FeOB (Neubauer et al., 2002), but may also result from their transport from the upstream aerator without active growth.

4.2. MOB activity shifts Fe removal from biotic to abiotic

The oxidation of iron was complete in the first filter of both systems (i.e., SF and TF), yet it was likely dominated by different processes. Strong indications of biological iron oxidation were found at genomic and proteomic levels in the SF. Bacteria of the genus *Gallionella* dominated the filter based on 16S rRNA gene amplicon sequencing (Fig. 5) and MAG-centric metagenomic analyses (Fig. 6), and the iron oxidation protein Cyc2 was homogeneously distributed across the filter depth (Fig. 8). Contrastingly, bacteria (Figs. 5 and 6) and genes (Fig. S5) related to iron oxidation were found at much lower relative abundances in the TF, and iron-oxidizing proteins were below the detection limit. Since the SF and TF featured a comparable total protein abundance (a proxy for biomass concentration; Table S2) and treated the same Fe load, these results suggest that biological Fe oxidation played a comparably

smaller role in the TF.

Only few studies report the application of trickling filters for drinking water production from groundwater, and biological oxidation is generally suggested to be the dominant iron removal mechanism, contributing to 35-65 % of total iron removal (see (Van Beek et al., 2016) and references therein). In terms of dissolved oxygen concentration and pH, the two main parameters known to control the prevailing iron oxidation mechanism (Müller et al., 2024; Van Beek et al., 2016), the reported values of pH 7.4 – 7.5 and DO > 8 mg O_2 L^{-1} are in the same range as in our system. As both TF and SF were operated at the same filtration velocity of 5 m h^{-1}, the fact that this velocity is higher than in published systems is unlikely to explain the total suppression of biological iron removal. Instead, we hypothesize the difference to reside either in limitations in micronutrients such as Cu or in oxygen availability. While the former has already been proposed and proven for ammonia oxidizers for conventional submerged filters (Wagner et al., 2016), the latter has not. The oxidation of 1 mg CH_4 demands 4 mg O_2, and groundwater contains 5 mg CH_4 L^{-1} and up to 10 mg O_2 L^{-1} after aeration. Since the diffusion coefficients of methane and oxygen are similar (see SI 8 for details), oxygen may be stoichiometrically limiting in the biofilm already for methane oxidation alone. In either case, MOB are likely outcompeting FeOB in the TF, owing to their higher biomass and energy yield per mol of oxygen. The observed full removal of iron is thus mainly ascribed to chemical reactions. Previous work on methane and iron co-removal concluded that the presence of methane itself does not interfere with overall iron removal (Grohmann et al., 1989; de Vet et al., 2002). Our results further confirm that complete iron removal can be attained in the presence of methane, while also revealing the induced shift from (partially) biological to chemical processes.

4.3. MOB outcompete AOB, and potentially directly contribute to ammonium removal

The presence of methane affects ammonium oxidation in the trickling filter. Complete ammonium removal was observed in the SF, while only partial conversion occurred in the TF (<20 %). In this filter, AOB were hardly found at 16S rRNA gene level, and the ammonia monooxygenase was not detected in the metagenome (Fig. 7B) or metaproteome (Fig. 8). Above, we attributed the very low abundance of ammonia oxidizers, including both canonical AOB and comammox *Nitrospira*, in the TF to the competition for oxygen and micronutrients such as Cu, combined with their lower growth yield compared to MOB. In analogy, while AOB feature a similar energy yield per electron as MOB, their biomass yields remain significantly lower. Consistently, *ex-situ* batch tests revealed a very low maximum ammonia oxidation capacity of the filter medium from top section of the TF (0.26 g NH_4^+-N m_{media}^{-3} h^{-1}) compared not only to the SF medium (1.83 g NH_4^+-N m_{media}^{-3} h^{-1}), but also to methane-free filters evaluated elsewhere (1.42 g NH_4^+-N m_{media}^{-3} h^{-1} (Tatari et al., 2016), 4.5 g NH_4^+-N m_{media}^{-3} h^{-1} (Corbera-Rubio et al., 2023), and 3-10 g NH_4^+-N m_{media}^{-3} h^{-1} (Lee et al., 2014)). Nevertheless, the *ex-situ* maximum ammonia oxidation rate of the TF medium increased 4-fold in the presence of CH_4 (Fig. 4A), suggesting that MOB may play a primary role in ammonium removal.

The ability of MOB to oxidize ammonia has been reported for decades and is attributed to the structural similarity between methane and ammonia, and the substrate promiscuity of methane monooxygenases (Bodelier and Frenzel, 1999; Bédard and Knowles, 1989). Ammonia oxidation by MOB can only yield hydroxylamine, nitric oxide, or nitrite as products (Versantvoort et al., 2020). Consistently, no nitrate was produced by the TF medium, while we clearly observed nitrate production from nitrification in *ex-situ* batch tests with the nitrifier-dominated SF medium. Growth of MOB on ammonium alone has never been reported, leading to the generally accepted assumption that MOB do not conserve energy from ammonia oxidation (Martikainen, 2022), which may partially explain the low ammonia oxidation rate by TF medium in the absence of methane. Still, the mechanism by which methane promotes ammonia oxidation by MOB warrants further research.

Ex-situ maximum ammonia oxidation rates were the highest in the ATF. The fact that filters devoid of iron have higher maximum ammonium removal capacities than filters reveiving iron has already been observed (Corbera-Rubio et al., 2023) and is suggested to relate to the inhibition of AOB by Fe^{3+} flocs, a product of homogeneous Fe^{2+} oxidation (Corbera-Rubio et al., 2024b). Interestingly, the ATF mainly contained nitrifiers associated with the genera *Nitrosomonas* (AOB) and *Candidatus* Nitrotoga (NOB), while the SF was dominated by *Nitrospira,* the most commonly found nitrifier in rapid sand filters (Gülay et al., 2016; Albers et al., 2015; Poghosyan et al., 2020). The observed prevalence of canonical *Nitrospira* in the SF and the higher relative abundances of NOB over AOB in all filters investigated here (Table S6) is consistent with most sand filter studies (Poghosyan et al., 2020; Fowler et al., 2018; Hu et al., 2020). While this is generally attributed to the dominance of comammox *Nitrospira*, the most abundant *Nitrospira* MAGs obtained from the SF metagenomes (SF1 and SF2) lacked *amoA,* and were not phylogenetically affiliated with comammox *Nitrospira*. The dominance of nitrite-oxidizing bacteria over ammonia oxidizers points to a more prominent role of their metabolic flexibility in rapid sand filters, a question to be further explored.

4.4. MOB activity delays Mn removal despite sufficient surface catalytic potential

Manganese was fully removed in both the submerged and trickling system, yet with stark differences. The SF removed >99 %, while the TF contributed less than 15 % to the total manganese removal. Interestingly, genes related to manganese oxidation were similarly distributed across all filters. Biological manganese oxidation is reported to play a minor role compared to chemical processes in mature filters (Breda et al., 2019a; Bruins et al., 2015), although recent work challenges this view (Haukelidsaeter et al., 2024). The transition from biological to chemical-dominated manganese oxidation has been reported to occur after less than 2 months (Breda et al., 2019b) to several years (Sahabi et al., 2009). Both the SF and TF were operated for approximately a year and the lack of detected known manganese-oxidizing proteins supports the prevalence of chemical reactions, in analogy to our previous work (Corbera-Rubio et al., 2023). Surprisingly, *ex-situ* incubation tests of the filter medium grains indicated that the manganese removal potentials of the SF and TF are comparable, excluding the lack of catalytic capacity as a reason for the incomplete removal in the TF. Manganese oxidation in sand filters starts only after complete iron and ammonium removal, as was the case for the SF (Fig. S4; (Corbera-Rubio et al., 2023)). In analogy, we hypothesize that iron (either as Fe^{2+} or Fe^{3+} flocs) penetrated deeper into the TF than the SF and that the resulting increased oxygen demand delayed the onset of manganese oxidation. Alternatively, the delay could relate to a possible accumulation of nitrite due to ammonia oxidation by MOB instead of complete nitrification, known to interfere with manganese oxidation (Cheng et al., 2017). Still, as Mn was fully removed in the following ATF, our results show that the implementation of a trickling filter for methane removal does not hinder full Mn removal in subsequent rapid sand filtration systems.

4.5. Implications for drinking water treatment

Biological methane removal through trickling biofiltration offers a promising approach for drinking water companies to meet increasingly stringent emission standards. For the largest drinking water company in the Netherlands, methane emissions from water extraction account for 14 % of the company's total CO_2-equivalent emissions (Vitens, 2022). Considering methane's 100-year Global Warming Potential (GWP) of 27 (IPCC, 2022), widespread implementation of this method can potentially mitigate up to 8,547 tonnes of CO_2-equivalent emissions annually for this company alone. This supports global efforts to reduce

greenhouse gas emissions and offers significant economic benefits. Based on the current European Union's Emissions Trading Scheme (EU ETS) carbon pricing of €69.51 per tonne (https://climate.ec.europa.eu/eu-action/eu-emissions-trading-system-eu-ets_en), this could translate to an annual cost saving of approximately €600,000.

In this study, 47 % of the groundwater methane was removed biologically in the trickling filter. Achieving complete biological removal is the natural next step to decrease the environmental impact of rapid sand filtration. We hypothesize that an increased water retention time in the filter will likely enhance methane removal. This could be achieved, for instance, by increasing the bed height or decreasing the water flow. To this end, the impact of the resulting water-to-air ratio (currently at 1:4 in forced co-current flow) on striping and oxygen availability, and on the potential delay of ammonium removal will also need to be assessed. When ammonia is not oxidized in the first filtration step, the second (and last) filter becomes the sole barrier to remove it, leaving the plant without any redundancy to tackle possible ammonium (and manganese) breakthroughs. In an earlier study, the biological stability of this plant was already investigated (de Vet et al., 2023), and the produced water was of excellent quality as efficient ammonium removal took place in the second filtration step. A small part of the ammonium was already removed in the first filter, hence an increased water retention times may further stimulate ammonia oxidation, potentially yielding a more robust process. Ultimately, while biological methane oxidation holds promise to effectively reduce the C-footprint of drinking water production, the extent of the impact on the stability of other (a)biotic processes and of the produced drinkingwater remain to be fully explored.

5. Conclusions

The implementation of a full-scale trickling filter prior to an existing submerged sand filter halved methane emissions by promoting biological methane oxidation. The novel process scheme also fully removed iron, ammonium, and manganese, yet the underlying mechanisms differed significantly from the parallel submerged filters preceded by conventional aeration. Methane-oxidizing bacteria outcompeted ammonia oxidizers, which only proliferated in the subsequent submerged filter, and MOB likely contributed directly to ammonia removal in the trickling filter. Signatures of biological iron oxidation were much less abundant in the trickling filter, suggesting that MOB also outcompeted iron oxidizers in this filter. In contrast to the submerged filters devoid of methane, the observed complete removal of iron during trickling filtration is therefore ascribed largely to chemical reactions. The reasons for the absence of manganese removal in the trickling filter, despite similar *ex-situ* manganese oxidation capacities, remain to be elucidated. Ultimately, our results demonstrate that trickling filtration may be highly effective in reducing methane emissions while achieving comparable effluent qualities, potentially playing a pivotal role in the transition towards more sustainable, resource-efficient groundwater treatment systems.

CRediT authorship contribution statement

Francesc Corbera-Rubio: Writing – original draft, Methodology, Investigation, Data curation, Conceptualization. **Alje S. Boersma:** Writing – original draft, Methodology, Investigation, Formal analysis, Data curation, Conceptualization. **Weren de Vet:** Writing – review & editing, Methodology, Investigation, Formal analysis, Conceptualization. **Martin Pabst:** Writing – review & editing, Investigation, Formal analysis, Data curation. **Paul W.J.J. van der Wielen:** Writing – review & editing, Supervision, Formal analysis. **Maartje A.H.J. van Kessel:** Writing – review & editing, Supervision, Methodology, Formal analysis, Conceptualization. **Mark C.M. van Loosdrecht:** Writing – review & editing, Supervision, Formal analysis, Conceptualization. **Doris van Halem:** Writing – review & editing, Supervision, Project administration, Methodology, Formal analysis, Conceptualization. **Sebastian Lücker:** Writing – review & editing, Supervision, Project administration, Methodology, Formal analysis, Conceptualization. **Michele Laureni:** Writing – review & editing, Supervision, Methodology, Formal analysis, Conceptualization.

Declaration of competing interest

The authors declare the following financial interests/personal relationships which may be considered as potential competing interests: Francesc Corbera-Rubio reports financial support was provided by Vitens NV. Francesc Corbera-Rubio reports financial support was provided by Dunea Duin & Water. Alje Boersma reports financial support was provided by Vitens NV. Alje Boersma reports financial support was provided by Dunea Duin & Water. If there are other authors, they declare that they have no known competing financial interests or personal relationships that could have appeared to influence the work reported in this paper.

Acknowledgments

The authors would like to thank Dita Heikens for the metaproteomic analysis and Hanna Koch for aiding in the phylogenetic analysis of NxrA/NarG. This work was financed by the NWO partnership program 'Dunea–Vitens: Sand Filtration' (projects 17830 and 17841) of the Dutch Research Council (NWO) and the drinking water companies Vitens NV and Dunea Duin & Water. ML, MvK, SL, and DvH were supported by NWO (project numbers VI.Veni.192.252, 016.Veni.192.062, 016.Vidi.189.050, and Vidi 18369, respectively).

Supplementary materials

Supplementary material associated with this article can be found, in the online version, at doi:10.1016/j.watres.2025.123450.

Data availability

Data will be made available on request.

References

Van der Aa, L.T.J., Kors, L.J., Wind, A.P.M., Hofman, J.A.M.H., Rietveld, L.C., 2002. Nitrification in rapid sand filter: phosphate limitation at low temperatures. In: Water Science and Technology: Water Supply, 2. IWA Publishing, pp. 37–46. https://doi.org/10.2166/ws.2002.0005.

Afshin, Y., Delherbe, N., Kalyuzhnaya, M.G., 2021. Methylotenera. Bergey's Manual of Systematics of Archaea and Bacteria. John Wiley & Sons, Ltd, pp. 1–11. https://doi.org/10.1002/9781118960608.gbm02021.

Albers, C.N., Ellegaard-Jensen, L., Harder, C.B., Rosendahl, S., Knudsen, B.E., Ekelund, F., Aamand, J., 2015. Groundwater chemistry determines the prokaryotic community structure of waterworks sand filters. Environ. Sci. Technol. 49 (2), 839–846. https://doi.org/10.1021/es5046452.

Alneberg, J., B.S. Bjarnason, I. Bruijn, M. Schirmer, J. Quick, UZ. Ijaz, NJ. Loman, AF. Andersson, and C. Quince. 2013. "CONCOCT: Clustering CONtigs on COverage and ComposiTion," December. https://arxiv.org/abs/1312.4038v1.

Bédard, C., Knowles, R., 1989. Physiology, biochemistry, and specific inhibitors of CH4, NH4+, and CO oxidation by methanotrophs and nitrifiers. Microbiol. Rev. 53 (1), 68. https://doi.org/10.1128/MR.53.1.68-84.1989.

Beek, C.G.E.M.V, Dusseldorp, J., Joris, K., Huysman, K., Leijssen, H., Schoonenberg Kegel, F., De Vet, W.W.J.M., Van De Wetering, S., Hofs, B., 2016. Contributions of homogeneous, heterogeneous and biological iron(II) oxidation in aeration and rapid sand filtration (RSF) in field sites. J. Water Supply Res. Technol. AQUA 65 (3), 195–207. https://doi.org/10.2166/aqua.2015.059.

Bodelier, P.L.E., Frenzel, P., 1999. Contribution of methanotrophic and nitrifying bacteria to CH4 and NH4+ oxidation in the rhizosphere of rice plants as determined by new methods of discrimination. Appl. Environ. Microbiol. 65 (5), 1826–1833. https://doi.org/10.1128/AEM.65.5.1826-1833.1999.

Bourgine, F.P., Gennery, M., Chapman, J.I., Kerai, H., Green, J.G., Rap, R.J., Ellis, S., Gaumard, C., 1994. Biological processes at saints hill water-treatment plant, kent. Water Environ. J. 8 (4), 379–391. https://doi.org/10.1111/j.1747-6593.1994.tb01121.x.

Bowers, R.M., Kyrpides, N.C., Stepanauskas, R., Harmon-Smith, M., Doud, D., Reddy, T. B.K., Schulz, F., et al., 2017. Minimum information about a single amplified genome (MISAG) and a metagenome-assembled genome (MIMAG) of bacteria and archaea. Nat. Biotechnol. 35 (8), 725–731. https://doi.org/10.1038/NBT.3893.

Breda, I.L., Ramsay, L., Søborg, D.A., Dimitrova, R., Roslev, P., 2019a. Manganese removal processes at 10 groundwater fed full-scale drinking water treatment plants. Water Qual. Res. J. Can. 54 (4), 326–337. https://doi.org/10.2166/wqrj.2019.006.

Breda, I.L., Søborg, D.A., Ramsay, L., Roslev, P., 2019b. Manganese removal processes during start-up of inoculated and non-inoculated drinking water biofilters. Water Qual. Res. J. 54 (1), 47–56. https://doi.org/10.2166/wqrj.2018.016.

Bruins, J.H., Petrusevski, B., Slokar, Y.M., Huysman, K., Joris, K., Kruithof, J.C., Kennedy, M.D., 2015. Biological and physico-chemical formation of birnessite during the ripening of manganese removal filters. Water Res. 69 (0), 154–161. https://doi.org/10.1016/j.watres.2014.11.019.

Buchfink, B., Xie, C., Huson, D.H., 2014. Fast and sensitive protein alignment using DIAMOND. Nat. Methods 12 (1), 59–60. https://doi.org/10.1038/NMETH.3176. *2014 12:1*.

Callahan, B.J., Paul, J., McMurdie, M.J., Rosen, A.W., Han, A., Johnson, J.A., Holmes, S. P., 2016. DADA2: high-resolution sample inference from illumina amplicon data. Nat. Methods 13 (7), 581–583. https://doi.org/10.1038/nmeth.3869. *2016 13:7*.

Caporaso, J.G., Lauber, C.L., Walters, W.A., Berg-Lyons, D., Huntley, J., Fierer, N., Owens, S.M., et al., 2012. Ultra-high-throughput microbial community analysis on the illumina HiSeq and MiSeq platforms. ISME J. 6 (8), 1621–1624. https://doi.org/10.1038/ismej.2012.8. *2012 6:8*.

Chaumeil, P.A., Mussig, A.J., Hugenholtz, P., Parks, DH., 2022. GTDB-Tk v2: memory friendly classification with the genome taxonomy database. Bioinformatics 38 (23), 5315–5316. https://doi.org/10.1093/BIOINFORMATICS/BTAC672. *Oxford, England*.

Cheng, Q., Nengzi, L., Xu, D., Guo, J., Yu, J., 2017. Influence of nitrite on the removal of Mn(II) using pilot-scale biofilters. J. Water Reuse Desalin. 7 (3), 264–271. https://doi.org/10.2166/wrd.2016.210.

Chklovski, A., Parks, D.H., Woodcroft, B.J., Tyson, G.W., 2023. CheckM2: a rapid, scalable and accurate tool for assessing microbial genome quality using machine learning. Nat. Methods 20 (8), 1203–1212. https://doi.org/10.1038/s41592-023-01940-w. *2023 20:8*.

Corbera-Rubio, F., Goedhart, R., Laureni, M., Loosdrecht, M.C.M., Halem, D., 2024a. A biotechnological perspective on sand filtration for drinking water production. Curr. Opin. Biotechnol. 90, 103221. https://doi.org/10.1016/J.COPBIO.2024.103221. December.

Corbera-Rubio, F., Kruisdijk, E., Malheiro, S., Leblond, M., Verschoor, L., Loosdrecht, M. C.M., Laureni, M., Halem, D., 2024b. A difficult coexistence: resolving the iron-induced nitrification delay in groundwater filters. Water Res. https://doi.org/10.1016/J.WATRES.2024.121923. June, 121923.

Corbera-Rubio, F., Laureni, M., Koudijs, N., Müller, S., Alen, T., Schoonenberg, F., Lücker, S., Pabst, M., Loosdrecht, M.C.M., Halem, D., 2023. Meta-omics profiling of full-scale groundwater rapid sand filters explains stratification of iron, ammonium and manganese removals. Water Res. 233, 119805. https://doi.org/10.1016/j.watres.2023.119805. April.

Cremers, G., Jetten, M.S.M., den Camp, H.J.M.O., Lücker, S., 2022. Metascan: METabolic Analysis, SCreening and ANnotation of metagenomes. Front. Bioinform. 2, 861505. https://doi.org/10.3389/FBINF.2022.861505/BIBTEX. June.

Daims, H., Lebedeva, E.V., Pjevac, P., Han, P., Herbold, C., Albertsen, M., Jehmlich, N., et al., 2015. Complete nitrification by nitrospira bacteria. Nature 528 (7583), 504–509. https://doi.org/10.1038/nature16461. *2015 528:7583*.

Edgar, R.C., 2004. MUSCLE: multiple sequence alignment with high accuracy and high throughput. Nucleic Acids Res. 32 (5), 1792. https://doi.org/10.1093/NAR/GKH340.

Eren, A.M., Kiefl, E., Shaiber, A., Veseli, I., Miller, S.E., Schechter, M.S., Fink, I., et al., 2020. Community-led, integrated, reproducible multi-omics with Anvi'o. Nat. Microbiol. 6 (1), 3–6. https://doi.org/10.1038/s41564-020-00834-3. *2020 6:1*.

Fowler, S.J., Palomo, A., Dechesne, A., Mines, P.D., Smets, B.F., 2018. Comammox nitrospira are abundant ammonia oxidizers in diverse groundwater-fed rapid sand filter communities. Environ. Microbiol. 20 (3), 1002–1015. https://doi.org/10.1111/1462-2920.14033.

Garber, A.I., Nealson, K.H., Okamoto, A., McAllister, S.M., Chan, C.S., Barco, R.A., Merino, N., 2020. FeGenie: a comprehensive tool for the identification of iron genes and iron gene neighborhoods in genome and metagenome assemblies. Front. Microbiol. 11, 37. https://doi.org/10.3389/fmicb.2020.00037.

González-Cabaleiro, R., Peter Curtis, T., Ofiţeru, I.D., 2019. Bioenergetics analysis of ammonia-oxidizing bacteria and the estimation of their maximum growth yield. Water Res. 154, 238–245. https://doi.org/10.1016/J.WATRES.2019.01.054. May.

Graham, E.D., Heidelberg, J.F., Tully, B.J., 2017. Binsanity: unsupervised clustering of environmental microbial assemblies using coverage and affinity propagation. PeerJ 2017 (3), e3035. https://doi.org/10.7717/PEERJ.3035/SUPP-5.

Grohmann, A., Gollasch, R., Schuhmacher, G., 1989. Biological iron and manganese removal of a methane containing groundwater in speyer. Gas Wasserfach Wasser Abwasser 130 (9), 441–446.

Gülay, A., Musovic, S., Jørgen Albrechtsen, H., Al-Soud, W.A., Sørensen, SJ., Smets, BF., 2016. Ecological patterns, diversity and core taxa of microbial communities in groundwater-fed rapid gravity filters. ISME J. 10 (9), 2209–2222. https://doi.org/10.1038/ismej.2016.16.

Hanson, R.S., Hanson, T.E., 1996. Methanotrophic bacteria. Microbiol. Rev. 60 (2), 439–471. https://doi.org/10.1128/MR.60.2.439-471.1996.

Haukelidsaeter, S., Boersma, A.S., Kirwan, L., Corbetta, A., Gorres, I.D., Lenstra, W.K., Schoonenberg, F.K., et al., 2023. Influence of filter age on Fe, Mn and NH4+ removal in dual media rapid sand filters used for drinking water production. Water Res. 242, 120184. https://doi.org/10.1016/j.watres.2023.120184. December 2022.

Haukelidsaeter, S., Boersma, A.S., Piso, L., Lenstra, W.K., Helmond, N.A.G.M.V., Schoonenberg, F., Pol, E.V.D., et al., 2024. Efficient chemical and microbial removal of iron and manganese in a rapid sand filter and impact of regular backwash. Appl. Geochem. 162, 105904. https://doi.org/10.1016/j.apgeochem.2024.105904. December 2023.

Herlemann, D.P.R., Labrenz, M., Jürgens, K., Bertilsson, S., Waniek, J.J., Andersson, A.F., 2011. Transitions in bacterial communities along the 2000 Km salinity gradient of the baltic sea. ISME J. 5 (10), 1571–1579. https://doi.org/10.1038/ismej.2011.41. *2011 5:10*.

Hu, W., Liang, J., Ju, F., Wang, Q., Liu, R., Bai, Y., Liu, H., Qu, J., 2020. Metagenomics unravels differential microbiome composition and metabolic potential in rapid sand filters purifying surface water versus groundwater. Environ. Sci. Technol. 54, 5206. https://doi.org/10.1021/acs.est.9b07143.

Hyatt, D., Liang Chen, G., LoCascio, P.F., Land, M.L., Larimer, F.W., Hauser, L.J., 2010. Prodigal: prokaryotic gene recognition and translation initiation site identification. BMC Bioinform. 11 (1), 1–11. https://doi.org/10.1186/1471-2105-11-119/TABLES/5.

Jiang, H., Chen, Y., Jiang, P., Zhang, C., Smith, T.J., Colin Murrell, J., Xing, X.H., 2010. Methanotrophs: multifunctional bacteria with promising applications in environmental bioengineering. Biochem. Eng. J. 49 (3), 277–288. https://doi.org/10.1016/j.bej.2010.01.003.

Kang, D.D., Li, F., Kirton, E., Thomas, A., Egan, R., An, H., Wang, Z., 2019. MetaBAT 2: an adaptive binning algorithm for robust and efficient genome reconstruction from metagenome assemblies. PeerJ 2019 (7). https://doi.org/10.7717/peerj.7359.

Kessel, M.A.H.J.V., Speth, D.R., Albertsen, M., Nielsen, P.H., Camp, H.J.M.O.D., Kartal, B., Jetten, M.S.M., Lücker, S., 2015. Complete nitrification by a single microorganism. Nature 528 (7583), 555–559. https://doi.org/10.1038/nature16459. *2015 528:7583*.

Kleikamp, H.B.C., Grouzdev, D., Schaasberg, P., van Valderen, R., van der Zwaan, R., van de Wijgaart, R., Lin, Y., et al., 2023. Metaproteomics, metagenomics and 16S RRNA sequencing provide different perspectives on the aerobic granular sludge microbiome. Water Res. 246, 120700. https://doi.org/10.1016/J.WATRES.2023.120700. November.

Kleikamp, H.B.C., Pronk, M., Tugui, C., Silva, L.G., Abbas, B., Lin, Y.M., Loosdrecht, M.C. M., Pabst, M., 2021. Database-independent de novo metaproteomics of complex microbial communities. Cell Syst. 12 (5), 375–383. https://doi.org/10.1016/J.CELS.2021.04.003 e5.

Knief, C., 2015. Diversity and habitat preferences of cultivated and uncultivated aerobic methanotrophic bacteria evaluated based on PmoA as molecular marker. Front. Microbiol. https://doi.org/10.3389/fmicb.2015.01346. Frontiers Media S.A.

Koch, H., Kessel, M.A.H.J., Lücker, S., 2019. Complete nitrification: insights into the ecophysiology of comammox nitrospira. Appl. Microbiol. Biotechnol. https://doi.org/10.1007/s00253-018-9486-3.

Leak, D.J., Dalton, H., 1986. Growth yields of methanotrophs–1. Effect of copper on the energetics of methane oxidation. Appl. Microbiol. Biotechnol. 23 (6), 470–476. https://doi.org/10.1007/BF02346062.

Lee, C.O., Boe-Hansen, R., Musovic, S., Smets, B., Albrechtsen, H.J., Binning, P., 2014. Effects of dynamic operating conditions on nitrification in biological rapid sand filters for drinking water treatment. Water Res. 64, 226–236. https://doi.org/10.1016/j.watres.2014.07.001 m.

Letunic, I., Bork, P., 2021. Interactive tree of life (ITOL) v5: an online tool for phylogenetic tree display and annotation. Nucleic Acids Res. 49 (W1), W293–W296. https://doi.org/10.1093/NAR/GKAB301.

Li, H., B. Handsaker, A. Wysoker, T. Fennell, J. Ruan, N. Homer, G. Marth, G. Abecasis, and R. Durbin. 2009. "The sequence alignment/map format and SAMtools" 25 (16): 2078–79. 10.1093/BIOINFORMATICS/BTP352.

Ludwig, W., Strunk, O., Westram, R., Richter, L., Meier, H., Yadhukumar, A., Buchner, A., et al., 2004. ARB: a software environment for sequence data. Nucleic Acids Res. 32 (4), 1363–1371. https://doi.org/10.1093/NAR/GKH293.

Malashenko, Y.R., Pirog, T.P., Romanovskaya, V.A., Sokolov, I.G., Grinberg, T.A., 2001. Search for methanotrophic producers of exopolysaccharides. Appl. Biochem. Microbiol. 37 (6), 599–602. https://doi.org/10.1023/A:1012307202011.

Martikainen, P.J., 2022. Heterotrophic nitrification–an eternal mystery in the nitrogen cycle. Soil Biol. Biochem. 168, 108611. https://doi.org/10.1016/j.soilbio.2022.108611. September 2021.

McMurdie, P.J., Holmes, S., 2013. Phyloseq: an R package for reproducible interactive analysis and graphics of microbiome census data. PLoS ONE 8 (4), e61217. https://doi.org/10.1371/JOURNAL.PONE.0061217.

Minh, B.Q., Schmidt, H.A., Chernomor, O., Schrempf, D., Woodhams, MD., Haeseler, A. V., Lanfear, R., Teeling, E., 2020. IQ-TREE 2: new models and efficient methods for phylogenetic inference in the genomic era. Mol. Biol. Evol. 37 (5), 1530–1534. https://doi.org/10.1093/MOLBEV/MSAA015.

Müller, S., F. Corbera-Rubio, F. Schoonenberg-Kegel, M. Laureni, M.C.M.V. Loosdrecht, D.V. Halem, M.C.M. Loosdrecht, and D. Halem. 2024. "Shifting to biology promotes highly efficient iron removal in groundwater filters." BioRxiv, February, 2024.02.14.580244. 10.1101/2024.02.14.580244.

Murreil, J.C., Gilbert, B., McDonald, I.R., 2000. Molecular biology and regulation of methane monooxygenase. Arch. Microbiol. 173 (5–6), 325–332. https://doi.org/10.1007/s002030000158.

Na, P.J., Yaramala, S.R., Kim, J.A., Kim, H., Goes, F.S., Zandi, P.P., Voort, J.L.V, Sutor, B., Croarkin, P., Bobo, W.V., 2018. The PHQ-9 item 9 based screening for suicide risk: a validation study of the patient health questionnaire (PHQ)-9 item 9 with the Columbia suicide severity rating scale (C-SSRS). J. Affect. Disord. 232, 34–40. https://doi.org/10.1016/J.JAD.2018.02.045. May.

Neubauer, S.C., Emerson, D., Patrick Megonigal, J., 2002. Life at the energetic edge: kinetics of circumneutral iron oxidation by lithotrophic iron-oxidizing bacteria isolated from the wetland-plant rhizosphere. Appl. Environ. Microbiol. 68 (8), 3988–3995. https://doi.org/10.1128/AEM.68.8.3988-3995.2002.

Nurk, S., Meleshko, D., Korobeynikov, A., Pevzner, P.A., 2017. MetaSPAdes: a new versatile metagenomic assembler. Genome Res. 27 (5), 824–834. https://doi.org/10.1101/GR.213959.116/-/DC1.

Palomo, A., Fowler, S.J., Gülay, A., Rasmussen, S., Sicheritz-Ponten, T., Smets, B.F., 2016. Metagenomic analysis of rapid gravity sand filter microbial communities suggests novel physiology of Nitrospira Spp. ISME J. 10 (11), 2569–2581. https://doi.org/10.1038/ismej.2016.63.

Poghosyan, L., Koch, H., Frank, J., Kessel, M.A.H.J., Cremers, G., Alen, T., Jetten, M.S.M., Camp, H.J.M.O., Lücker, S., 2020. Metagenomic profiling of ammonia- and methane-oxidizing microorganisms in two sequential rapid sand filters. Water Res. 185, 116288. https://doi.org/10.1016/j.watres.2020.116288. October.

Price, M.N., Dehal, P.S., Arkin, A.P., 2010. FastTree 2 – approximately maximum-likelihood trees for large alignments. PLoS ONE 5 (3), e9490. https://doi.org/10.1371/JOURNAL.PONE.0009490.

Quast, C., Pruesse, E., Yilmaz, P., Gerken, J., Schweer, T., Yarza, P., Peplies, J., Glöckner, F.O., 2013. The SILVA ribosomal RNA gene database project: improved data processing and web-based tools. Nucleic Acids Res. 41. https://doi.org/10.1093/NAR/GKS1219. Database issue.

Sahabi, D.M., Takeda, M., Suzuki, I., Koizumi, J., 2009. Removal of Mn2+ from water by 'aged' biofilter media: the role of catalytic oxides layers. J. Biosci. Bioeng. 107 (2), 151–157. https://doi.org/10.1016/j.jbiosc.2008.10.013.

Sander, R., 2015. Compilation of Henry ' s law constants for water as solvent, version. Atmos. Chem. Phys. Discuss. https://doi.org/10.5194/acpd-14-29615-2014, 29615–521.

Shaffer, M., Borton, M.A., McGivern, B.B., Zayed, A.A., Leanti La Rosa, S., Solden, LM., Liu, P., et al., 2020. DRAM for distilling microbial metabolism to automate the curation of microbiome function. Nucleic Acids Res. 48 (16), 8883–8900. https://doi.org/10.1093/NAR/GKAA621.

Sieber, C.M.K., Probst, A.J., Sharrar, A., Thomas, B.C., Hess, M., Tringe, S.G., Banfield, J. F., 2018. Recovery of genomes from metagenomes via a dereplication, aggregation and scoring strategy. Nat. Microbiol. 3 (7), 836–843. https://doi.org/10.1038/s41564-018-0171-1. *2018 3:7*.

Søborg, D.A., Breda, I.L., Ramsay, L., 2015. Effect of oxygen deprivation on treatment processes in a full-scale drinking water biofilter. Water Sci. Technol. Water Supply 15 (4), 825–833. https://doi.org/10.2166/ws.2015.040.

Stanley, S.H., Prior, S.D., Leak, D.J., Dalton, H., 1983. Copper stress underlies the fundamental change in intracellular location of methane mono-oxygenase in methane-oxidizing organisms: studies in batch and continuous cultures. Biotechnol. Lett. 5 (7), 487–492. https://doi.org/10.1007/BF00132233.

Stein, L.Y., Roy, R., Dunfield, P.F., 2012. Aerobic methanotrophy and nitrification: processes and connections. eLS. https://doi.org/10.1002/9780470015902.a0022213 no. 2011.

Tatari, K., Smets, B.F., Albrechtsen, H.J., 2016. Depth investigation of rapid sand filters for drinking water production reveals strong stratification in nitrification biokinetic behavior. Water Res. 101, 402–410. https://doi.org/10.1016/j.watres.2016.04.073. September.

Trifinopoulos, J., Nguyen, L.T., Haeseler, A., Minh, B.Q., 2016. W-IQ-TREE: a fast online phylogenetic tool for maximum likelihood analysis. Nucleic Acids Res. 44, W232–W235. https://doi.org/10.1093/NAR/GKW256. W1.

Versantvoort, W., Pol, A., Jetten, M.S.M., van Niftrik, L., Reimann, J., Kartal, B., Op den Camp, H.J.M., 2020. Multiheme hydroxylamine oxidoreductases produce NO during ammonia oxidation in methanotrophs. Proc. Natl. Acad. Sci. USA 117 (39), 24459–24463. https://doi.org/10.1073/pnas.2011299117.

Vet, W., Advies, H., Burger, W., Advies, H., Woerdt, D.V.A.N.D.E.R., Advies, H., 2002. Methane load irrelevant for filter performance. H2O 35 (1), 26–29.

Vet, W., Van Genuchten, C.C.A., Van Loosdrecht, M.C.M., Van Dijk, J.C., 2010. Water quality and treatment of river bank filtrate. Drink. Water Eng. Sci. 3 (1), 79–90. https://doi.org/10.5194/dwes-3-79-2010.

Vet, W., Rietveld, L.C., Van Loosdrecht, M.C.M., 2009. Influence of iron on nitrification in full-scale drinking water trickling filters. J. Water Supply Res. Technol. AQUA 58 (4), 247–256. https://doi.org/10.2166/aqua.2009.115.

Vitens. 2022. "2022 annual report every drop sustainable".

Wagner, F.B., Nielsen, P.B., Boe-Hansen, R., Albrechtsen, H.J., 2016. Copper deficiency can limit nitrification in biological rapid sand filters for drinking water production. Water Res. 95, 280–288. https://doi.org/10.1016/j.watres.2016.03.025.

Wu, Y.W., Simmons, B.A., Singer, S.W., 2016. MaxBin 2.0: an automated binning algorithm to recover genomes from multiple metagenomic datasets. Bioinformatics 32 (4), 605–607. https://doi.org/10.1093/bioinformatics/btv638.